Naval Research Laboratory

Washington, DC 20375-5320

NRL/MR/5675--20-10,117

Modeling and Experimental Verification of Longitudinal Modes in Distributed Bragg Reflector Fiber Lasers

Gary A. Miller

Optical Techniques Branch
Optical Sciences Division

August 4, 2020

REPORT DOCUMENTATION PAGE

Form Approved
OMB No. 0704-0188

1. REPORT DATE *(DD-MM-YYYY)*	2. REPORT TYPE	3. DATES COVERED *(From - To)*
00-00-2020	NRL Memorandum Report	

4. TITLE AND SUBTITLE

Modeling and Experimental Verification of Longitudinal Modes in Distributed Bragg Reflector Fiber Lasers

5a. CONTRACT NUMBER

5b. GRANT NUMBER

5c. PROGRAM ELEMENT NUMBER
62747N

6. AUTHOR(S)

Gary A. Miller

5d. PROJECT NUMBER
UW-747-021

5e. TASK NUMBER
T051-16

5f. WORK UNIT NUMBER
6A36

7. PERFORMING ORGANIZATION NAME(S) AND ADDRESS(ES)

Naval Research Laboratory
4555 Overlook Avenue, SW
Washington, DC 20375-5320

8. PERFORMING ORGANIZATION REPORT NUMBER

NRL/MR/5675--20-10,117

9. SPONSORING / MONITORING AGENCY NAME(S) AND ADDRESS(ES)

Office of Naval Research
One Liberty Center
875 N Randolf Street, Suite 1425
Arlington, VA 22203-1995

10. SPONSOR / MONITOR'S ACRONYM(S)

ONR

11. SPONSOR / MONITOR'S REPORT NUMBER(S)

12. DISTRIBUTION / AVAILABILITY STATEMENT

DISTRIBUTION STATEMENT A: Approved for public release; distribution is unlimited.

13. SUPPLEMENTARY NOTES

14. ABSTRACT

Little, if any, experimental data exists that explores how different design characteristics affect the number of longitudinal modes in extended cavity fiber lasers. To help facilitate the design of distributed Bragg reflector (DBR) lasers, a numerical model was used to synthesize their response to various design modifications such as grating reflectivity and bandwidth. Lasers were then fabricated, characterized and compared to the computer model. Experiments were also conducted to determine how the longitudinal mode structure changed depending on the amount of gain available in the laser cavity and where the gain medium was placed within the cavity. These experiments determined the optimum combination of a fiber Bragg grating's (FBG) reflectivity/bandwidth and gain necessary to produce a stable DBR fiber laser. Experiments were then conducted to determine the spectral offset (through grating strain) needed to achieve single longitudinal mode (SLM) lasing in DBR fiber lasers under a variety of conditions. Simulations were used to confirm and calculate the influence of the FBG coupling strength and length, strain, cavity length, and laser threshold. Analytical expressions using these parameters were derived and used to verify experimental data and predict the performance of subsequent laser designs.

15. SUBJECT TERMS

Fiber Bragg grating
Fiber Laser
Modeling
Longitudinal mode structure

16. SECURITY CLASSIFICATION OF:			17. LIMITATION OF ABSTRACT	18. NUMBER OF PAGES	19a. NAME OF RESPONSIBLE PERSON
a. REPORT	b. ABSTRACT	c. THIS PAGE			Gary A. Miller
Unclassified Unlimited	Unclassified Unlimited	Unclassified Unlimited	Unclassified Unlimited	32	19b. TELEPHONE NUMBER *(include area code)* (202) 767-9510

Standard Form 298 (Rev. 8-98)
Prescribed by ANSI Std. Z39.18

This page intentionally left blank.

CONTENTS

MODELING AND EXPERIMENTAL VERIFICATION OF LONGITUDINAL MODES IN DISTRIBUTED BRAGG REFLECTOR FIBER LASERS

1. INTRODUCTION

Sensors based on fiber lasers can resolve displacements less than a femtometer because their frequency stability is limited by intrinsic thermodynamic noise, achieving this fundamentally-limited strain resolution with cavities lengths from less than one centimeter to a few meters using interferometric demodulation. Highly stable distributed feedback (DFB) fiber lasers obtain this resolution with effective cavity lengths of a few millimeters, whereas interferometric-based fiber sensors require more than 100 times this length. This high sensitivity per unit lengths makes fiber laser sensors (FLS) well-suited for compact sensor arrays.

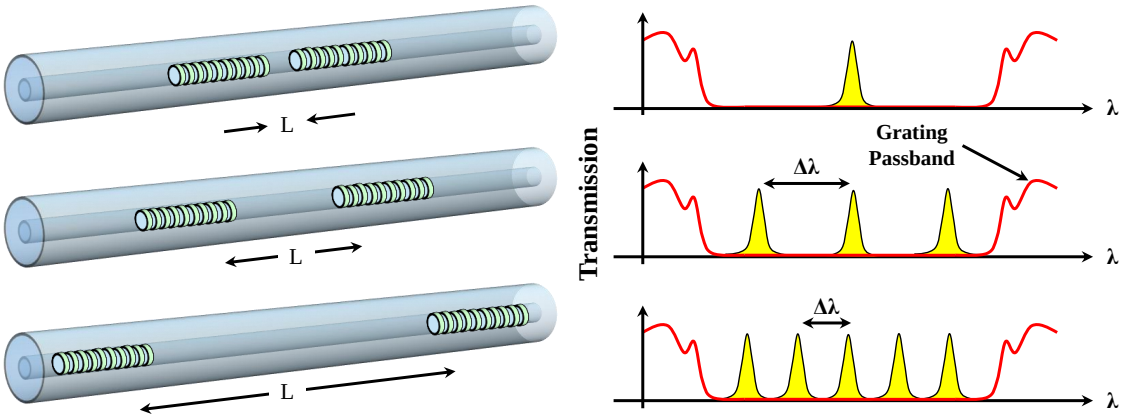

Fig. 1—(Left) DBR fiber lasers of various cavity lengths with their corresponding longitudinal mode structure (Right).

If longer interaction lengths are required, distributed Bragg reflector (DBR) fiber lasers can be utilized. In this design, a pair of fiber Bragg gratings (FBGs) defines a linear laser cavity. The basic design of a DBR laser is illustrated in Fig. 1. The length between the gratings can be increased to provide spatial sampling of the sensing environment. However, as the cavity length increases, the laser begins to support multiple longitudinal modes (as seen to the right in Fig. 1). The mode spacing is given by $\Delta\nu = c/(2nL)$ in frequency or $\Delta\lambda = \lambda^2/(2nL)$ in wavelength, where ν is the laser frequency, λ is the laser wavelength, n is the effective index of the fiber, and L is the cavity length. While it would be reasonable to surmise that the cavity length is defined by the edges of the gratings, the cavity length is actually longer because the light penetrates some distance through the grating before it is reflected back into the cavity. Typically, the stronger the FBG, the shorter the penetration. For uniform gratings, the effective length of the grating is given by

$$L_{eff} = \frac{1}{2\kappa}\tanh(\kappa L_{FBG}), \tag{1}$$

Manuscript approved July 15 2020.

where κ is the magnitude of the coupling coefficient, and L_{FBG} is the length of the grating [1]. For apodized gratings, a scale factor (ξ) can be inserted such that κL, the integrated coupling coefficient (ICC), becomes $\xi\kappa L$ [2]. The scale factor represents the normalized integrated apodization profile such that for uniform gratings, ξ is 1. Not surprisingly, for weak gratings L_{eff} is $L/2$, or half the grating's length.

While any strain applied to the extended cavity causes all longitudinal modes to shift their frequency in unison, interferometric demodulation requires the path imbalance of the interferometer to be an integer multiple of the laser cavity length. This is often challenging to achieve. Thus, new designs that exploit the variety of grating properties are necessary to produce lasers that operate with a single longitudinal mode (SLM). The idea is illustrated in Fig. 2, whereby the grating parameters are adjusted such that only an SLM is permitted to operate. This provides an additional element of wavelength selectivity that can reduce the number of modes.

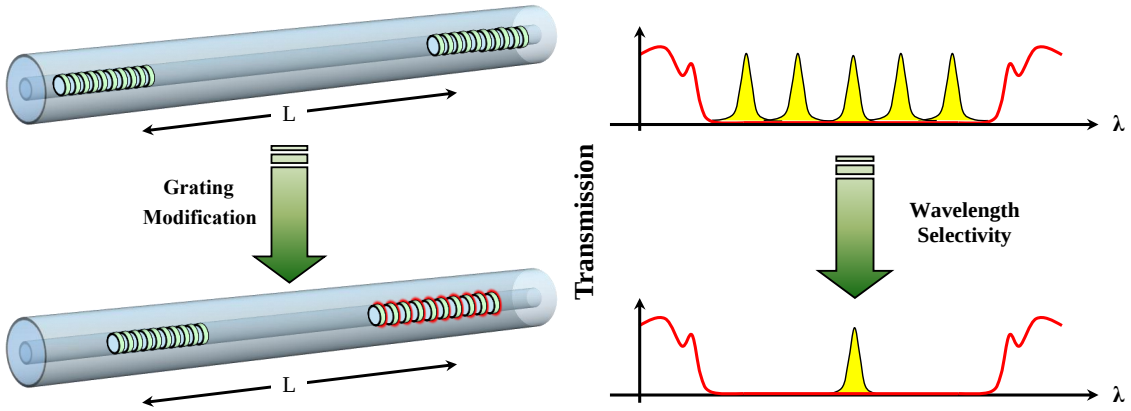

Fig. 2—(Left) Modification of the DBR laser design to permit single longitudinal mode operation. (Right) Incorporating additional wavelength selectivity reduces the number of modes.

To help predict the performance of different laser designs, a numerical model was utilized to solve for the modes of DBR fiber lasers. The model is based on the transfer matrix approximation of the coupled mode equations, where an FBG is represented by matrices that describe the propagation of the electric field through the waveguide [3]. This method can be used to solve for the threshold condition and detuning of cavity modes [4]. For model verification, extended cavity fiber lasers were fabricated with lengths up to 1 m. The lasers were then characterized for their transmission, reflection, and emission spectra. Longitudinal mode beating was analyzed using an RF spectrum analyzer, and the output power and pump absorption were measured. Experiments were also conducted to determine how the longitudinal mode structure changed depending on the amount of gain available in the laser cavity and where the gain medium was placed within the cavity. The effect of grating reflectivity and bandwidth on the number of modes supported by a linear cavity was also measured. Spectral overlap between grating pairs was also examined as a method to limit the bandwidth available for longitudinal modes to exist [5]. Offset designs were simulated, and an analytical expression was derived that estimated the performance of the lasers. Several lasers were then fabricated to confirm the model. Combined with the other experiments, these measurements helped determine the parameters necessary to produce the longest linear cavity with sufficient gain to support a single longitudinal mode.

2. FIBER LASER MODEL

2.1 Longitudinal Modes

The model is based on the transfer matrix approximation of the coupled mode equations. Here, a grating is sliced into several piecewise continuous segments where each of the grating properties are kept constant within the section [3]. Each segment has a corresponding 2×2 transfer matrix associated with it describing the forward and backward propagating electric fields. The concatenation of these matrices generates a single 2×2 matrix representing the entire grating structure. The matrices can also be used to solve for the threshold condition and detuning of DFB and DBR fiber lasers [2, 4]. To do so, the program finds the resonance or oscillation condition when the reflected and transmitted amplitudes are zero. This occurs when the gain in the cavity equals the internal losses of the cavity. Because gain and loss are represented as imaginary terms in the propagation constant, the Muller method is used to find the complex roots for a given set of detuning values [6]. The method calculates the resultant grating matrix and searches for when the diagonal components are zero, yielding the detuning and threshold values. It is important to note that this model contains a few limitations: 1) it does not incorporate spatial hole burning or other effects that might limit the number of modes present in the cavity and 2) it does not account for modal competition that may give rise to mode partition noise and variations in the longitudinal mode amplitudes. Due to these restrictions, the model only calculates modes that can potentially exist in the laser cavity, not whether they actually do exist.

With short laser cavities, the number of modes can be approximated by noting the available gain in the laser cavity and the threshold of each mode. Additionally, a cutoff condition for the nearest neighbor modes is utilized. In other words, to determine the number of modes, the total threshold gain of all modes must equal the available gain in the fiber, and the next nearest mode must be less than or equal to some limiting value. In the experiments discussed later, the gain of the fiber is approximately 1.15 m^{-1} [2], but given variations in manufacturing tolerance, the available gain was set to 1.3 m^{-1}. For the second condition, the limiting value was set at 0.03 m^{-1}. This means that if a mode has a threshold of 0.01 m^{-1}, the next mode must have a threshold value within 0.03 m^{-1} (i.e. 0.04 m^{-1}).

For extended laser cavities, this approach is problematic because several longitudinal modes might exhibit the same low threshold values, close to 0 m^{-1}. To accommodate multiple modes with the same values, the criterion is switched to a “minimum modes” model. Here, the two lowest threshold modes are tallied to determine the total number of modes. This typically means that the threshold values were 0 m^{-1} and 0.01 m^{-1}. Although this rule was arbitrarily determined, it has some merit based on the observation that for short cavity lengths, the minimum threshold was regularly 0.01 m^{-1} for multiple modes rather than 0 m^{-1}. Thus, modes with threshold values of 0.01 m^{-1} were just as likely to lase as modes with values of 0 m^{-1}.

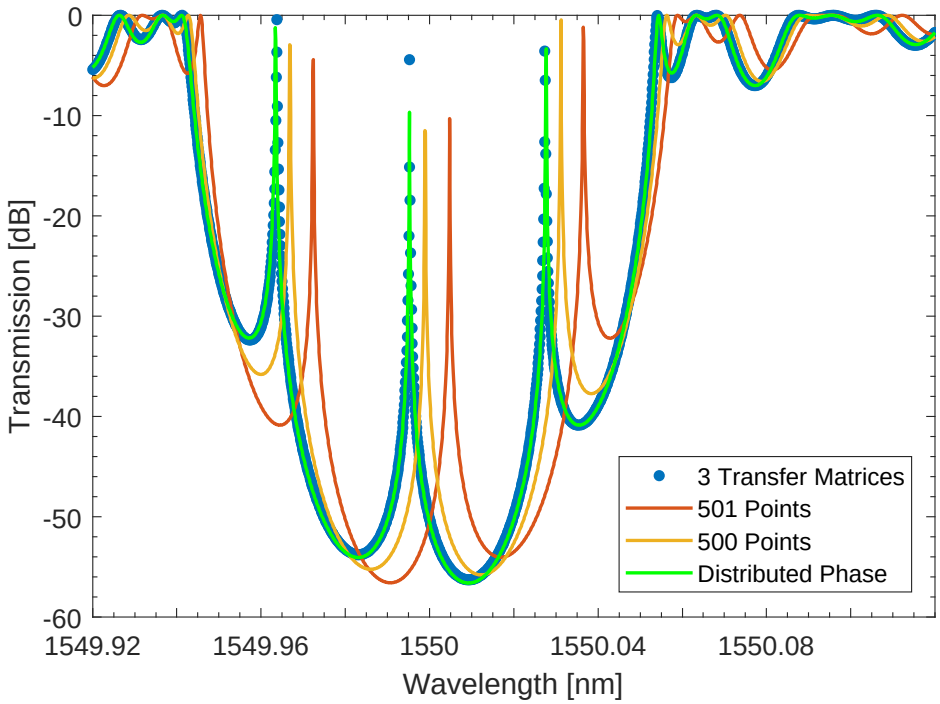

Fig. 3—Effect of discretization on the location of Fabry-Perot resonances in a 2 cm linear cavity DBR fiber laser.

2.2 Discretization of Laser Cavities

In order to simulate DBR designs, it is necessary to correctly account for the phase delay created by propagation through bare fiber. In the transfer matrix approximation, this is easily accomplished with a matrix of pure propagation (dependent on the length and effective index). However, in routines that rely on designating an arbitrary coupling coefficient along the length of the fiber, a different approach is required. The complex coupling coefficient is typically represented by [7]

$$|\kappa(z)| = \frac{\pi \eta \, \delta n_{ac}(z)}{\lambda_B} \text{ and} \tag{2}$$

$$\arg(\kappa(z)) = \theta(z) - \frac{4\pi\eta}{\lambda_B} \int_0^z \delta n_{dc}(z')dz' + \frac{\pi}{2}. \tag{3}$$

Here, λ_B is the nominal Bragg wavelength, η is the mode overlap factor, $\delta n_{dc}(z)$ is the slowly-varying index change, $\delta n_{ac}(z)$ is the index modulation amplitude, Λ is the period of the grating, z is the spatial coordinate along the fiber axis, and $\theta(z)$ is the excess phase due to grating period chirp and phase perturbations. If the grating experiences pure chirp, $\theta(z)$ can be described by

$$\theta(z) = \frac{4\pi\eta n_{eff}}{\lambda_B} \int_0^z \left(\frac{\lambda_B}{\lambda_D(z')} - 1 \right) dz'. \tag{4}$$

where n_{eff} is the effective index of the waveguide and $\lambda_D(z)$ is the local Bragg wavelength. To correctly account for the phase delay within the cavity, we can think of the local Bragg wavelength as approaching infinity within the region, such that Eq. (4) reduces to

$$\theta(z) = -\frac{4\pi\eta n_{eff}}{\lambda_B} \int_{z_1}^{z_2} dz', \tag{5}$$

where n_{eff} is integrated and evaluated over the bounds of the cavity (z_1 and z_2). This is akin to incorporating the phase term $e^{i\frac{2\pi}{\lambda_B} n_{eff} L_{cav}}$, where L_{cav} is the cavity length, in the transfer matrix.

In discretizing the coupling coefficient, it becomes evident that changes in dz' will change the phase of the cavity. The effect of quantization errors is illustrated in Fig. 3. Here, a Fabry-Perot cavity (comprised of two, 2 cm long uniform gratings with a 2 cm gap) is simulated under three conditions: 1) transfer matrix with three matrices including a pure propagation matrix utilizing the exact length of the cavity, 2) transfer matrix with a discretized coupling coefficient of 500 or 501 points, and 3) transfer matrix with a discretized coupling coefficient with the actual accumulated phase distributed over the discretized cavity length. Note that in case 1, only three matrices are required because the gratings used in this example are uniform, with no apodization. Thus, one matrix represents each FBG, and the cavity is represented by a single propagation matrix.

At 1550 nm and an effective index of 1.45, the 2 cm cavity experiences a phase delay (modulo 2π) of 2.23 rads (blue dots). If the entire structure is quantized with 501 sections, the closest cavity spacing is 1.992 cm, resulting in a phase delay of 4.26 rads (red line). Clearly this phase value is incorrect and as a result, does not properly model the resonance locations of the Fabry-Perot cavity. If the structure is quantized with 500 points (yellow line), the cavity length becomes 1.996 cm with a phase of 2.30 rads. While closer, this still does not accurately predict the resonances. To accommodate for errors related to the quantization, the correct phase delay is computed for the true cavity length and distributed over the discretized cavity (green line). This ensures that regardless of the number of sampled points, the phase delay due the cavity is correctly incorporated into the model.

3. EXTENDED CAVITY LASER DESIGN

Lasers of various lengths and parameters were fabricated using Nufern's PS-ESF erbium-doped optical fiber as the gain medium. Gratings were either written in the erbium-doped fiber or a mode-matched pigtail fiber (comprised of Nufern's PS-GSF optical fiber). For mode-matched samples, the splice loss between fibers was minimal and a conventional fusion splicer was utilized. For dissimilar fibers, additional splice joint processing was necessary to facilitate low loss splices [8]. To prepare the fibers for inscription, 30 mm of jacket was stripped using methylene chloride and placed in the fabrication setup [9].

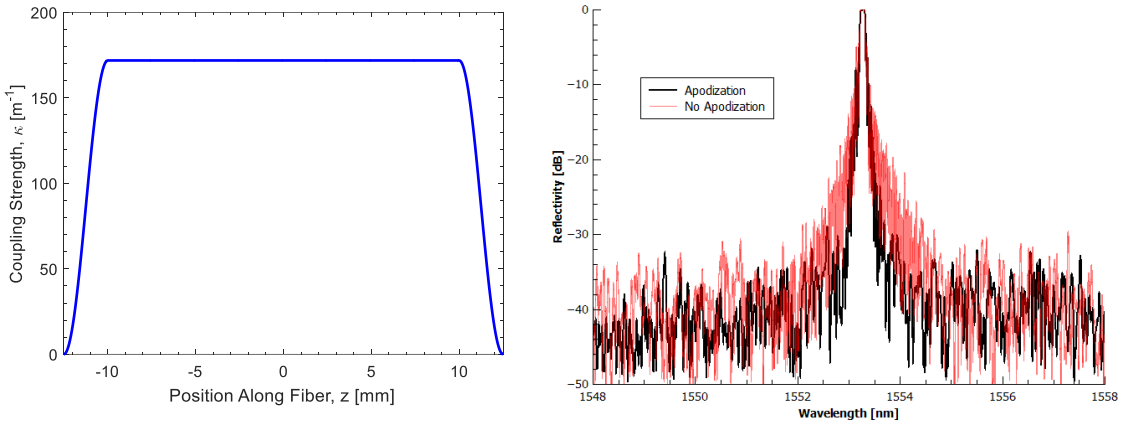

Fig. 4—(Left) Tapered cosine apodization profile used for gratings. (Right) Effect of apodization on the reflection spectrum.

The nominal grating design utilized a tapered cosine apodization profile, whereby a cosine function was used to dither the phase mask and reduce the fringe contrast over a given distance. Figure 4 illustrates a 10% taper such that 2.5 mm from each side of a 25 mm grating is affected ($\xi = 0.9$). Tapering the edges of the gratings suppresses the spectral response of side lobes and reduces the amount of out-of-band reflections. The figure to the right illustrates this point. The two gratings represented in this graph are nearly identical, with the exception that one employs a tapered cosine and the other is a uniform grating without any tapering of the grating profile. Clearly the grating design with apodization provides less reflection sensitivity to adjacent channels in a multiplexed system.

The gratings were written using 244 nm light with a Coherent Innova 300c MotoFreD in our in-house grating fabrication setup [9]. The fiber was exposed to an intensity of approximately 140 W/cm^2. To achieve a significant index change, the translation stage was moved at a speed of 0.03 mm/sec, equating to a fluence of 0.72 kJ/cm^2 [2]. Fluorescence tracking was utilized to keep the UV beam on the fiber during the exposure. The fiber was also held under a constant tension of 33 g. After the first grating was written and its transmission spectrum acquired, the fiber was shifted an amount and the second grating was exposed. Once the gratings were inscribed in the fiber, laser operation was verified by pumping the fiber at 980 nm (100 mW) and recording the emission spectrum on an optical spectrum analyzer (OSA). If the laser successfully lased, all exposed fiber was recoated and the grating transmission, reflection, and emission spectra were measured using a high resolution OSA from APEX Technologies. Note that a weak grating written in PS-ESF produces a reflection peak at 1553.5 nm. For a grating period of 535.5 nm, this yields an effective index of 1.4505.

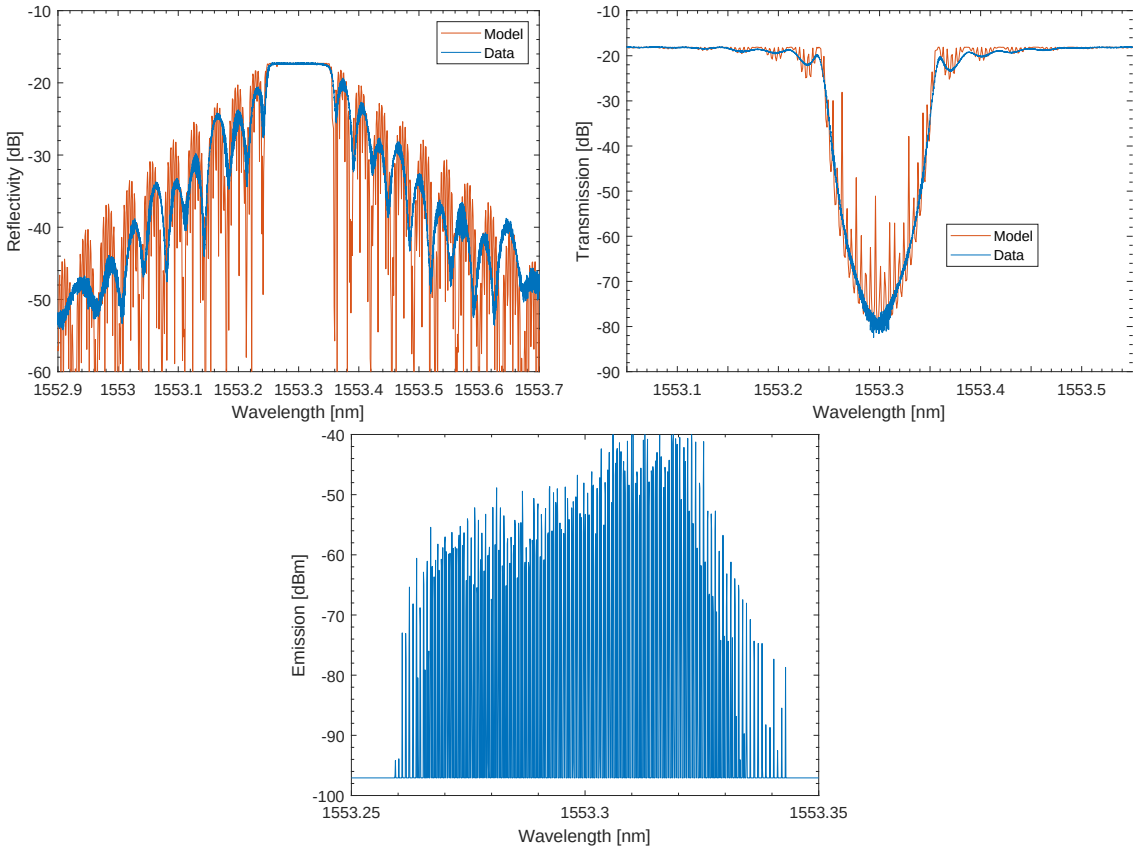

Fig. 5—(Left) Reflection, (Right) transmission, and (Bottom) emission spectra for a fiber laser with a cavity length of 1 m.

4. NUMBER OF MODES

The transmission, reflection, and emission spectra for a nominal laser with 1 m cavity are shown in Fig. 5. The total transmission is approximately 62 dB, and the bandwidth of the reflection spectrum is 0.12 nm (defined as the width between the "zeroes" on either side of the main Bragg peak). The emission spectrum was obtained by sending the backward propagating laser light through a WDM coupler and connecting the output to a high resolution OSA (Apex Technologies). The emission spectrum in Fig. 5 shows a significant amount of longitudinal modes present in the laser. Although the amplitudes of the modes fluctuate with time as environmental conditions change, the overall output power remains relatively constant. The longitudinal modes occupy 0.082 nm within the 0.12 nm bandwidth of the reflection spectrum. There are a total of 179 modes present (above a threshold of -80 dBm), including polarization modes. Further analysis of the emission spectrum reveals a mode spacing of 0.813 pm (101 MHz), equating to an effective cavity length of 1.027 m. The two polarization modes are spaced 0.325 pm apart (40 MHz). If the longitudinal modes were to occupy the entire FBG bandwidth, a total of 292 modes should exist, but considering the emission bandwidth is less (i.e. the extent of the viable longitudinal modes), the maximum number of modes drops to 202, near the number of modes shown in Fig. 5.

The plots in Fig. 5 also show a comparison between the spectral model and the acquired data. Some of the differences between traces are due to the instrument's resolution and dynamic range compared to the

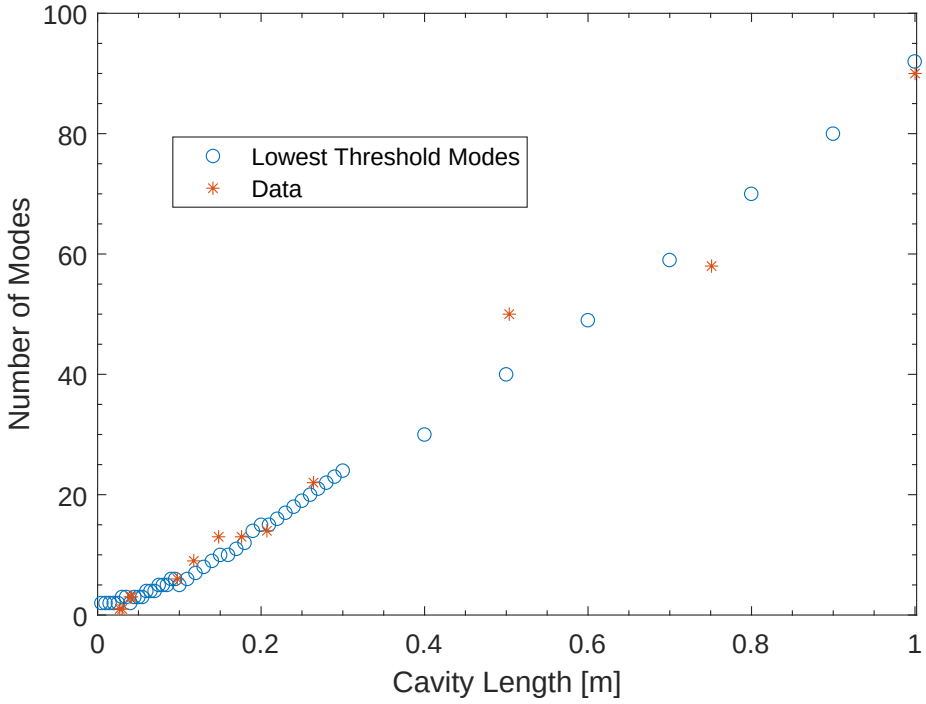

Fig. 6—Number of longitudinal modes versus cavity length for a DBR fiber laser. Simulated laser modes were determined using the "minimum modes" criterion.

arbitrary resolution assigned during the simulation. Discrepancies are also the result of imperfections in the phase mask encountered during the inscription process that lead to non-idealized grating spectra as a result of phase errors [9]. Additionally, strong gratings like the one in Fig. 5 exhibit complex refractive index profiles produced by higher-order interference effects near the phase mask that also affect the FBG spectra [10]. Despite these effects, the model simulates the reflection and transmission spectra adequately. The fiber laser model described earlier was also used to simulate the number of modes present in the laser cavity. Using the "minimum modes" criterion, the lowest threshold values are 0 m^{-1} and 0.1 m^{-1}, for a total of 92 longitudinal modes in a single polarization. The longitudinal mode spacing is 0.83 pm, close to the actual value of 0.81 pm. Taking both polarizations into account (simply doubling the value), the number of modes increases to 184, showing good agreement between the simulation and the reported number of longitudinal modes in the laser cavity (179).

4.1 Cavity Length

The model can also be used to estimate the number of modes as a function of the laser cavity length. This was achieved by sequentially adding increasingly larger gaps between the gratings, computing the spectra, solving for the laser mode thresholds, and using the "minimum modes" criterion to tabulate the total number of modes. As mentioned previously, careful attention was required to correctly quantize the distance between gratings due to the discrete step size and variable number of points spanning the gap. The number of modes were experimentally verified by performing a series of cutback measurements on the fiber laser. First, fiber was extracted from the center of the laser cavity through a series of cleaves. Then, the fiber was re-spliced ($<$ 0.04 dB per splice [8]) to restore the laser cavity. Afterwards, the laser was interrogated using the OSA to monitor the reflection, transmission, and emission spectra. Tension was applied to one FBG so that the

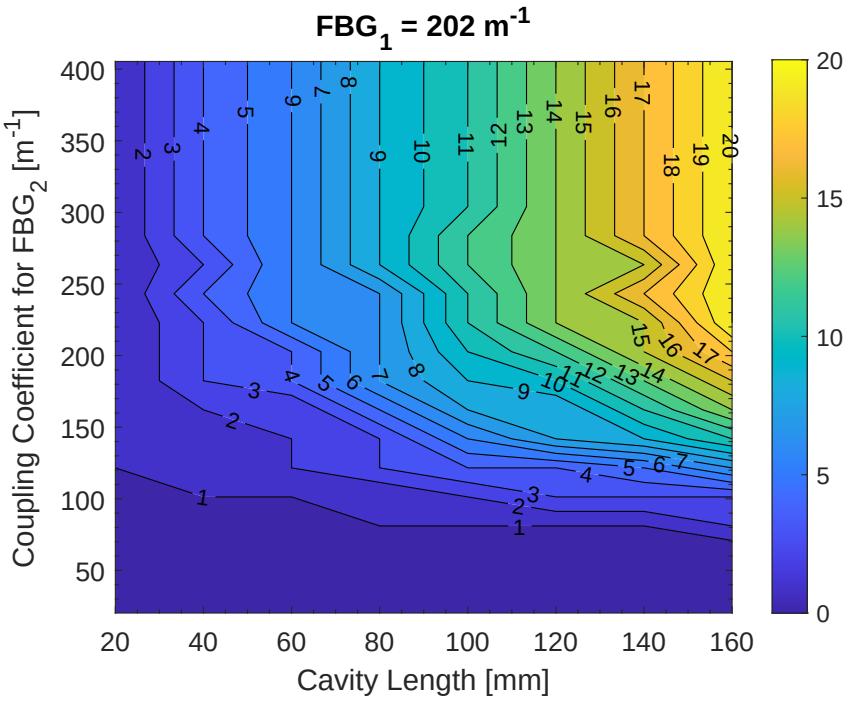

Fig. 7—Number of longitudinal modes (contours) for a DBR fiber laser versus cavity length and coupling coefficient of FBG_2. The coupling strength for FBG_1 was fixed at 202 m^{-1}, and simulated laser modes were determined using the "available gain" criterion.

resulting spectra exhibited maximum overlap of the individual grating spectra. The effective cavity length was then determined using the longitudinal mode spacing from the emission spectrum. Figure 6 shows the results from the cutback measurements overlaid with simulated data for a single polarization. The data and model are in good agreement. The results illustrate a linear trend of 93 modes/m for a single polarization starting at a cavity length of 10 cm. While there are some notable variations, other environmental factors such as the local temperature experienced by each grating can affect the modal structure, giving rise to variations in the output as a function of time. Thus at any given moment, the number of modes might fluctuate due to detuning of the gratings relative to one another. Mode hopping or modal competition can also affect the number of modes present in the cavity, causing certain modes to be suppressed at a given instance. Nonetheless, the model provides a faithful estimate of the number of modes for a given cavity length of this laser design.

To further understand how the number of modes relates to the cavity length of different laser designs, the model was used to simulate FBGs of varying lengths and coupling coefficients. In these simulations, the model employed 20 mm apodized gratings with 2 mm tapers and 16 mm flattops. The first grating (FBG_1) was set to an index modulation of 1×10^{-4} for a coupling coefficient of 202 m^{-1}. The second grating's index modulation (FBG_2) was varied from 1×10^{-5} to 20×10^{-5}, for a maximum coupling coefficient of 404 m^{-1}. The cavity length was also varied between 20 mm and 160 mm. Due to the shorter cavity lengths, the "available gain" criterion was instituted to calculate the number of modes (single polarization). The result of the computation is illustrated in Fig. 7 where the generated surface plot depicts the number of modes as a function of the cavity length and coupling coefficient of FBG_2. The figure illustrates that for κ values greater than 70 m^{-1}, the mode contours are relatively flat across all cavity lengths. However, once the

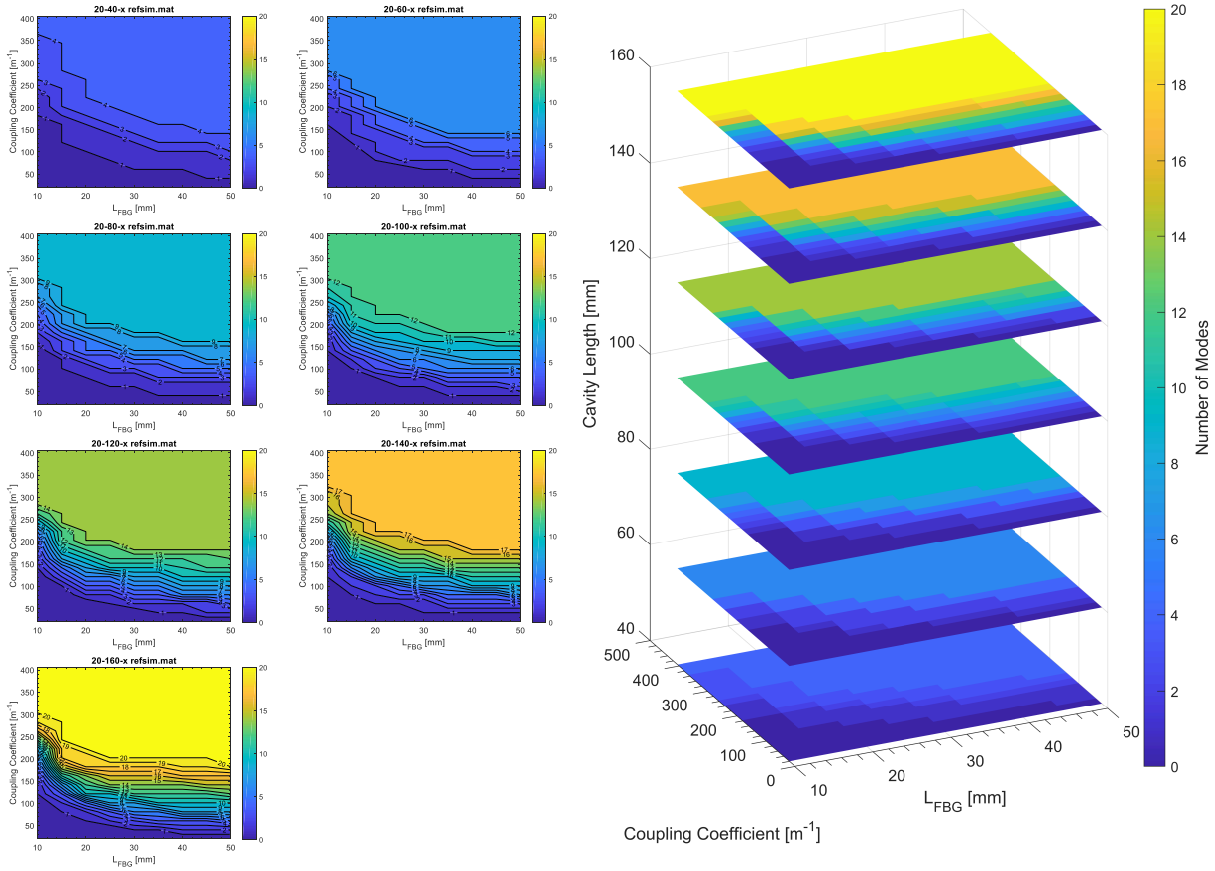

Fig. 8—(Left) Series of simulations showing the number of modes as a function of the coupling strength and length of FBG_2. The title of each subplot references the cavity length for the simulation (i.e. 20-40-x signifies a cavity length of 40 mm). (Right) Stacked representation of the data to the left illustrating the general trend of the simulation.

two gratings are equal in strength, the number of modes steadily increases with cavity length. Beyond 202 m^{-1}, the number of modes stays relatively constant for a fixed cavity length. This makes sense considering the grating with the smaller bandwidth will be a limiting factor in determining the number of modes that can be supported as will the amount of available gain. The figure can be of use in determining what laser design parameters might produce an SLM. For example, recall that the length of both gratings is 20 mm and apodized with scale factor of 0.9. To maintain an ICC of 7, FBG_2 must have a coupling coefficient of 187 m^{-1}. According to Fig. 7 in this example, the cavity length can be no longer than 30 mm if an SLM is desired.

The simulation can be parameterized further by varying the length of FBG_2 from 10 mm to 50 mm. In doing so, an estimation of how the length of the grating, and subsequently the grating bandwidth, affects the number of modes can be made (single polarization). As with the previous example, FBG_1 was 20 mm in length with a κ value of 202 m^{-1}. To ease the computational burden, the gratings were modeled with uniform profiles rather than tapered cosines. For a given cavity length, the length and strength of FBG_2 were swept, and the number of modes calculated. Then, the length of the cavity was increased, and the

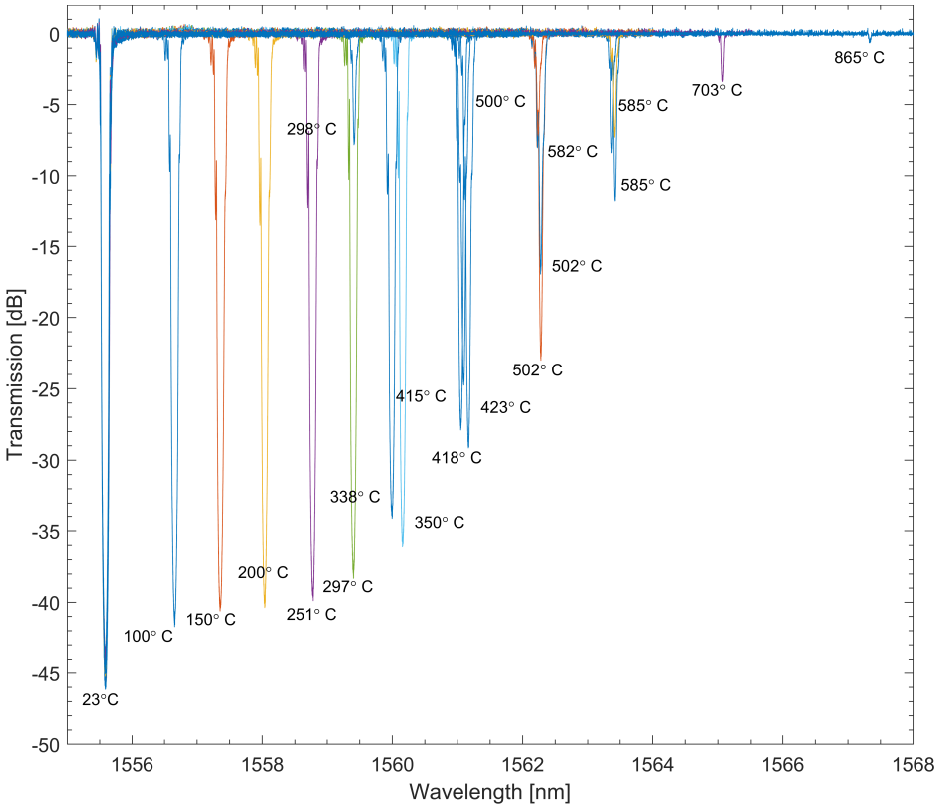

Fig. 9—Transmission spectra of FBG_2 at various stages of thermal processing. The left most spectra is FBG_1. [11]

grating parameters were varied again. The results of the simulations are shown in Fig. 8. As the cavity length increases, the mode fronts become compressed and flatter with respect to the grating length. The figures also show that there is a large plateau above which the number of modes is constant. This is due to FBG_1 ultimately limiting the spectral bandwidth the modes can occupy. With uniform FBGs, the bandwidth is dependent upon the reflectivity and grating length—the stronger the grating and the shorter it is, the wider the bandwidth. For gratings with different lengths but the same reflectivity, shorter gratings have wider bandwidths. Therefore in Fig. 8, the plateau indicates where the bandwidth of FBG_1 becomes less than FBG_2. From the plots, it is also apparent that for longer cavity lengths, the ability to operate in an SLM becomes increasingly challenging. The densely spaced contours illustrate the limited grating parameters that will suppress higher order modes. In practice, achieving such a tight tolerance on these factors is difficult, especially considering compositional variations along the length of fiber that can affect grating properties. The right plot in Fig. 8 depicts the data to the left in a stacked representation. The cavity length now becomes the vertical axis, demonstrating how the number of modes evolve over the entire parameter space.

4.2 Grating Reflectivity and Bandwidth

In another series of experiments, the effect of grating reflectivity and bandwidth on the number of modes supported by a linear cavity was measured. Nurfern's PS-GSF photosensitive fiber was used for the gratings, and PS-ESF erbium-doped fiber ($\sim$75 cm) provided gain for the 1 m laser cavity. The gratings were 25 mm in length, utilized the tapered cosine apodization profile mentioned previously, and had transmission values

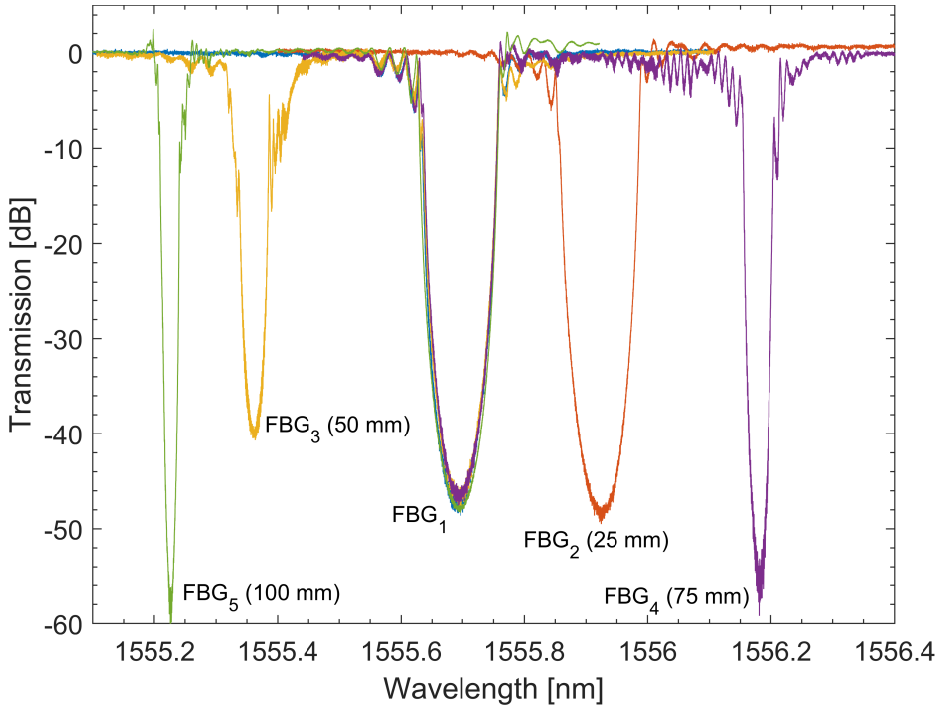

Fig. 10—Transmission spectra of several gratings used to determine the number of modes versus bandwidth. FBG_{2-5} were utilized to change the overall spectral bandwidth of the laser compared to bandwidth provided by FBG_1.

of 45 dB (FBG_1) and 41 dB (FBG_2). For reflectivity measurements, one grating (FBG_2) was sequentially thermally annealed (i.e. erased) inside a muffle furnace until the grating was too weak to provide feedback into the cavity ($>$ 700 °C) [11]. The grating spectra at each annealing step are shown in Fig. 9. After each thermal cycle, the oven was cooled to a slightly elevated temperature (100 °C), then FBG_1 was strain-tuned to overlap its reflection spectrum with the annealed spectrum. Finally, the transmission, reflection, and emission spectra were taken, noting the bandwidth and reflectivity of the grating. Note, the annealing experiments technically affected both the bandwidth and the reflectivity of the grating since both are related to the index modulation. The reflectivity of the FBG limits the number of modes by reducing the amount of optical feedback into the laser cavity. Unfortunately, it is difficult to create an experiment whereby the reflectivity of the grating is decreased and the bandwidth is held constant. The only way to achieve this scenario is to introduce a periodic chirp into the grating period to broaden the spectrum, a task currently beyond the capabilities of the fabrication setup. Therefore the results of this measurement include the combined effect of a reflectivity and bandwidth reduction.

To determine how the bandwidth alone affected the number of modes, several gratings of different lengths were written, then spliced onto the laser cavity to replace one of the original FBGs. The laser comprised two 2.5 cm gratings written in PS-GSF fiber and a cavity length of approximately 1 m of which 43 cm was erbium-doped fiber (PS-ESF). The transmission depths were 47.3 dB (FBG_1) and 48.8 dB (FBG_2) for each grating. The individual grating bandwidths were 0.135 nm and 0.141 nm for FBG_1 and FBG_2, respectively. To maintain similar reflectivities, the subsequent gratings were inscribed at increasingly faster scan rates so that the total fluence was constant. However, the gratings were often too strong and spectrally wide. To reduce the reflectivity and bandwidth, the gratings were annealed in the muffle furnace at 450 °C

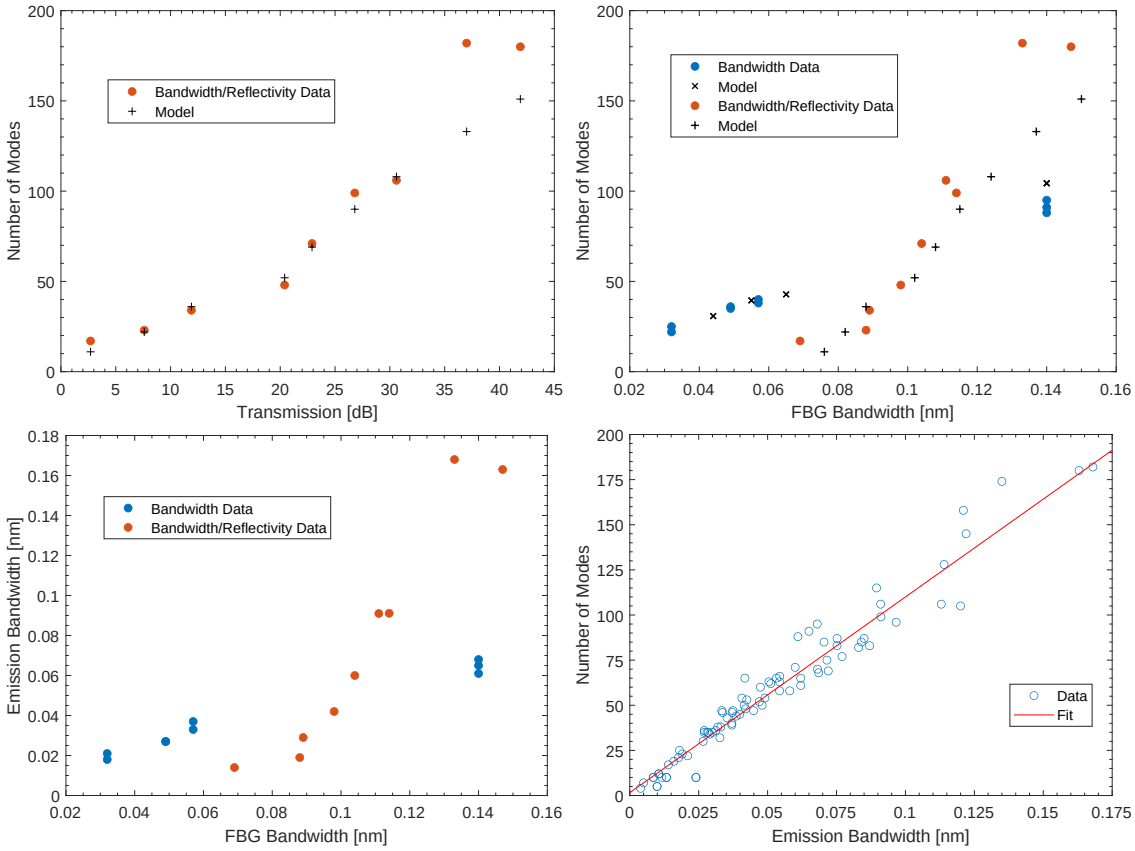

Fig. 11—(Top Left) Number of longitudinal modes versus transmission for a 1 m DBR fiber laser. (Top Right) Number of longitudinal modes versus grating bandwidth. The data reflects two experiments under different conditions for controlling the spectral bandwidth. (Bottom Left) Emission bandwidth versus grating bandwidth. (Bottom Right) Emission bandwidth versus the number of longitudinal modes. Note that simulated laser modes were determined using the "minimum modes" criterion.

for several minutes. The test gratings included FBGs with lengths 50 mm (FBG_3), 75 mm (FBG_4), and 100 mm (FBG_5). Transmission spectra of the various FBGs used in the tests are illustrated in Fig. 10. Although the reflectivities of the subsequent gratings varied from FBG_1 by upwards of 10 dB, they provide sufficient feedback to support the maximum number of longitudinal modes. Therefore, the spectral bandwidth of the grating limits the number of modes present in the cavity.

The model was used to predict the number of modes as FBG_2 was annealed or replaced with longer gratings using the "minimum modes" criterion. Figure 11 illustrates the number of longitudinal modes (single polarization) versus the grating transmission and bandwidth. The model and the data match well, showing a linear relationship between the number of modes and the strength of the second grating. In viewing the data of the first experiment, there is a slight divergence between the model and data set. This is possibly due to spectral sidelobes having enough reflectivity to support lasing or imperfect overlap between grating spectra. Because this laser action occurs outside the main lobe, the model does not incorporate these modes. Looking at the bandwidth data in Fig. 11, the model also compares well to the data. For both experimental sets, there is a linear relationship between the bandwidth and the number of modes. Of note however, is that the linear trends of the two data sets have differing slopes. The linear fit for the bandwidth only data is more gradual than for the annealed grating. Some of this behavior is due to the added effect of

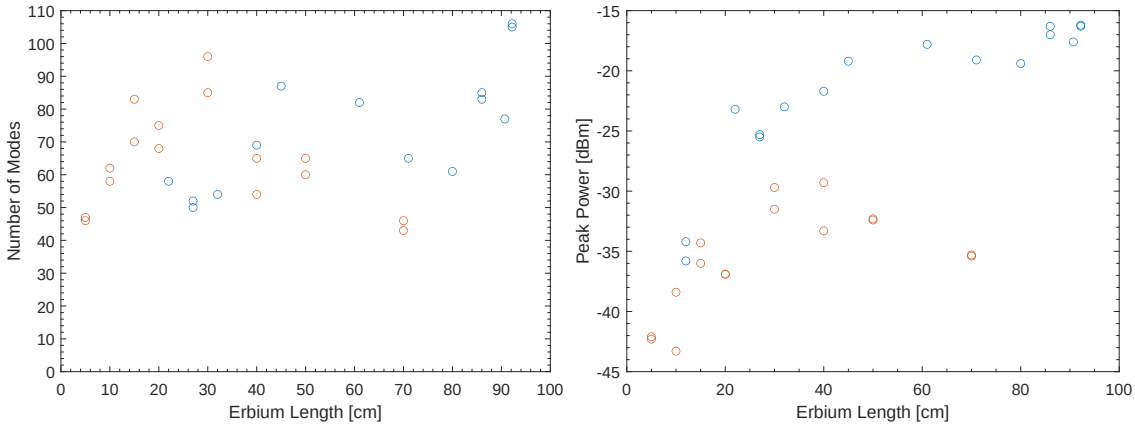

Fig. 12—(Left) Number of longitudinal modes and (Right) peak power versus erbium length. Blue circles denote when active fiber was replaced with passive fiber; red circles indicate when passive fiber was replaced by active fiber.

the change in the reflectivity of the grating. Since weaker gratings reduce the amount of feedback into the cavity, the number of modes should decrease at a faster rate. The behavior could also be due to the difference in the amount of erbium-doped fiber used to form the cavities for each experiment (75 cm versus 43 cm). Less fiber means there is less gain available for the higher order modes to reach threshold, and those that do lase will have significantly reduced power compared to lower order modes. The bottom left graph in Fig. 11 shows the emission bandwidth compared to the FBG bandwidth. The data also exhibits a linear relationship and demonstrates how the emission bandwidth is generally less than the grating bandwidth. The exception being the case when there is sufficient reflectivity in the sidelobes to allow for lasing outside the main Bragg stopband. The bottom right of Fig. 11 depicts the emission bandwidth versus the number of longitudinal modes. The data was aggregated from all experiments and exhibits a well-defined trend. Outliers are likely due to experimental error in the overlap of grating bandwidths and the difficulty in tabulating the modes. The linear response follows a slope of 1 mode/pm and has an offset of 1.6 modes.

4.3 Erbium-doped Fiber Length

Experiments were performed to determine if the length of erbium fiber affected the number of longitudinal modes. For this experiment, two lasers were fabricated: one comprised entirely from PS-ESF erbium-doped fiber and one from PS-GSF photosensitive fiber. The gratings were 2.5 cm long with a tapered cosine apodization profile. The transmission depths of the gratings were between 30 dB and 43 dB, with bandwidths between 0.12 nm to 0.14 nm. The cavity lengths of the lasers were 90 cm for the PS-ESF fiber and 100 cm for the PS-GSF fiber. Figure 12 shows the number of modes (single polarization) as a function of the length of erbium fiber in the cavity. In one experiment, successively longer pieces of active fiber were extracted from the center of the cavity and replaced with an equal length of PS-GSF fiber (blue circles). In the other experiment, the passive fiber in the center of the cavity was replaced with PS-ESF fiber (red circles). After the fibers were spliced, the laser characteristics were measured. The graphs in Fig. 12 reveal considerable variability in the data sets with little dependence on the fiber length. The scattering could be related to the difficulty in achieving perfect overlap between the gratings when pumped, but is also likely indicative of the minimal effect the erbium length has on the number of longitudinal modes. While the length of erbium doesn't appear to reduce the number of longitudinal modes, the right plot in Fig. 12 illustrates that it does dramatically reduce the peak optical power of the modes.

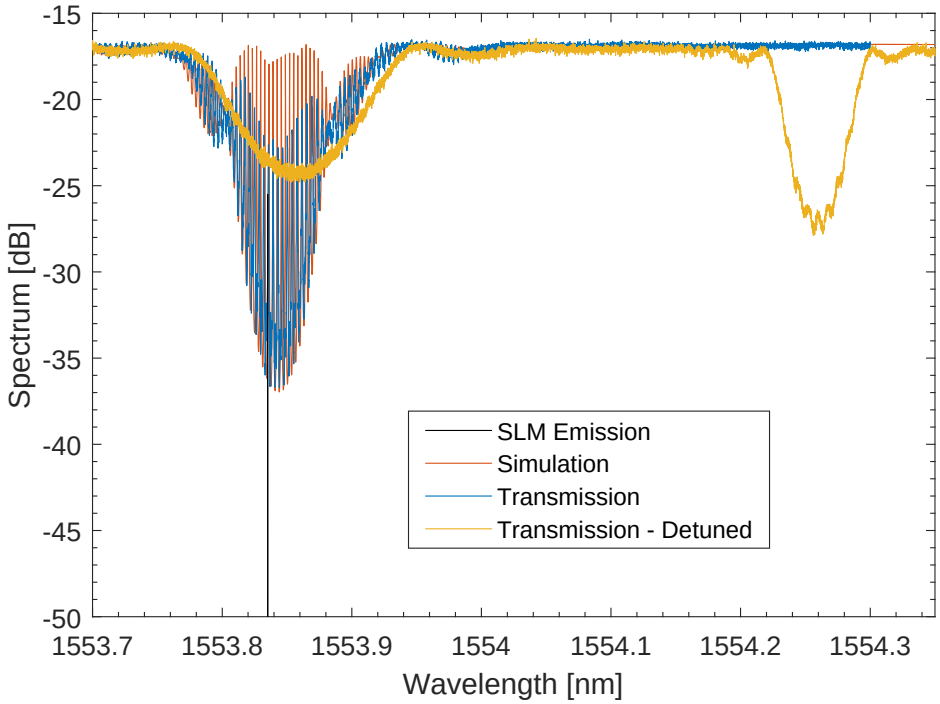

Fig. 13—Test DBR laser design for operating in an SLM. The detuned transmission spectrum shows the individual gratings that compose the cavity.

4.4 Test Laser Design

To further evaluate the influence of these design parameters on the formation of longitudinal modes, a test laser was constructed in which the reflectivity and bandwidth of the gratings were tailored to promote lasing in an SLM. The reflectivity was controlled by altering the scan speed during grating inscription, and the bandwidth was adjusted by extending the length of the grating. For this experiment, the target cavity length was 25 cm. The laser comprised two gratings written in PS-ESF optical fiber with lengths 25 mm (FBG_1) and 10 mm (FBG_2). The transmission depths of FBG_1 and FBG_2 were 10.8 dB and 7.5 dB, respectively. For FBG_1, the bandwidth was 84 pm, and for FBG_2, 189 pm. Modeling indicated that an SLM should be produced in the laser cavity with a threshold of 0.8 m^{-1}. Considering the gain of the fiber is 1.3 m^{-1}, the laser was expected to produce a weak output signal. Figure 13 illustrates the transmission and emission spectra for the laser. The gold trace shows the transmission spectrum with the gratings detuned from one another. The spectrum to the left centered around 1553.86 nm is FBG_2, evidenced by the broader width due to the shortened grating length. The overlapped spectrum is shown in blue. It exhibits a well-defined central lobe and two prominent side lobes. Because the bandwidth of FBG_1 is less than FBG_2, the central lobe is defined by the narrower resonance of FBG_1. The red line represents the spectrum generated by the laser simulation and matches the acquired spectrum well. When pumped, the test laser achieved lasing in an SLM (black line). The mode spacing was 3.45 pm, equating to an effective cavity length of 24.1 cm. As expected, the reduced grating reflectivities limited the optical feedback in the laser such that only -25.5 dBm of output power was produced. For higher output powers, stronger gratings or a longer cavity with more active fiber is needed. However, a redesign of the grating reflectors would also be needed if the laser is to operate in an SLM.

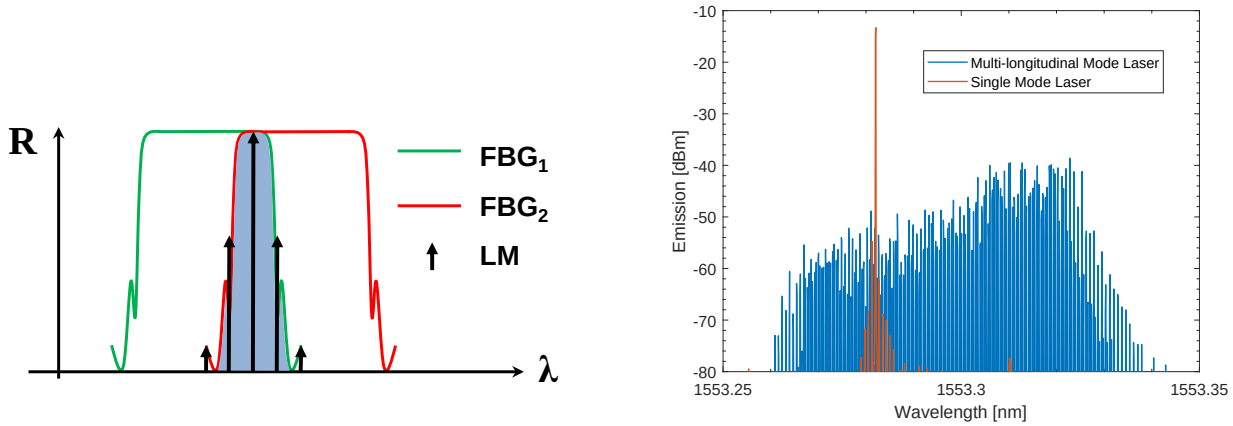

Fig. 14—(Left) Reduced spectral bandwidth (shaded region) created by modifying the period of one grating. (Right) SLM operation of 1 m cavity fiber laser using a spectral offset grating.

5. SINGLE LONGITUDINAL MODE OPERATION

An alternative approach to achieving SLM operation in a DBR fiber laser is to adjust one grating's spectrum relative to the other to reduce the spectral overlap. The resulting overlapped region effectively narrows the bandwidth available for longitudinal modes to exist. This point is illustrated in Fig. 14 where one grating's spectrum has been shifted to longer wavelengths. The black arrows represent the longitudinal modes present in the laser cavity. The height of the arrows gives an indication of the reflectivities of the Bragg gratings at the longitudinal mode locations. Modes with sufficient feedback (e.g. high enough reflectivity) will achieve lasing. The spectrum can be adjusted by index tuning the grating via an increase in the average refractive index (and ultimately the effective index) or modifying directly its Bragg period [5]. In adjusting the grating period to achieve SLM, there are a few points to consider: 1) when detuned, the overlapped reflectivity may decrease, making the laser more susceptible to back-reflection sensitivity, 2) any change in the detuning of the second grating could cause another longitudinal mode to appear, and 3) the grating's bandwidth and reflectivity will determine the amount of offset needed to produce an SLM.

To reliably determine the conditions for SLM generation, a fiber mount was created to detune one grating independent of the other. This permitted identical gratings to be utilized for determining the optimum spectral parameters needed to produce an SLM. Detuning was facilitated using a PI piezo stage (P-752.11c) with 15 µm of travel. A fiber clamp secured one end of the FBG to the stage while another secured the other end to a fixed platform. The stage was then actuated to strain the FBG. A large aluminum block provided a heat sink for the FBGs, helping to prevent thermal fluctuations from further detuning the gratings (due to environmental conditions or self-heating of the gratings). The FBGs were coupled to the block using thermal paste. Between gratings, the fiber was sandwiched between pieces of foam to limit thermal variations from changing the cavity length during measurements. For the experiment, one grating was detuned while pumped with a 980 nm laser diode. The output of the laser was analyzed using a spectrum analyzer and OSA. Single or few mode lasing was confirmed by monitoring the beat signals on a spectrum analyzer. The reflection and transmission spectra were also captured to observe where the emission line related to the grating spectra. Preliminary tests by stretching one grating in the fiber demonstrated the technique was viable for generating SLM fiber lasers. The plot to the right in Fig. 14 illustrates the collapse of the multiple modes into an SLM and the increase optical power from operating in an SLM. In this example, the nearest longitudinal mode is approximately 50 dB below the main peak.

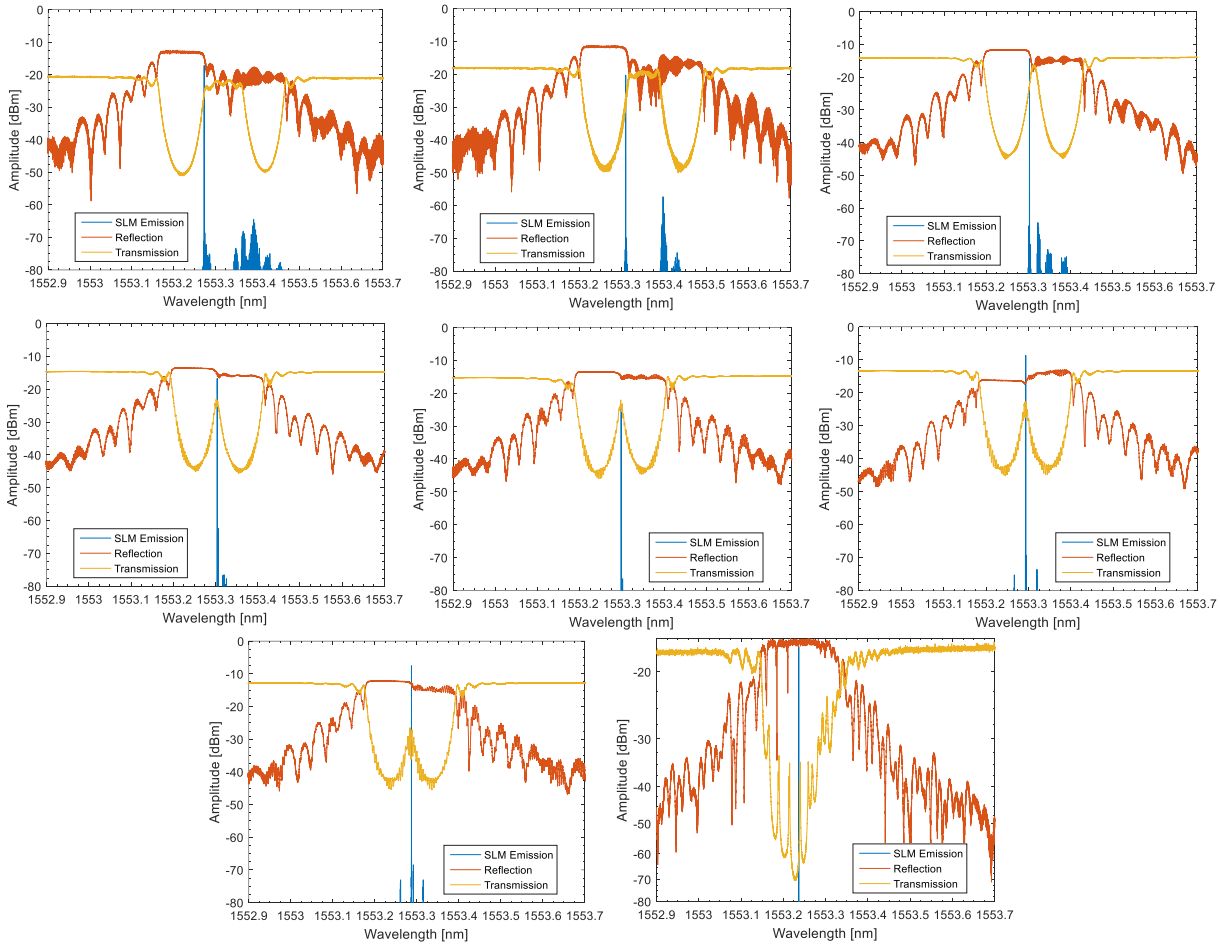

Fig. 15—Reflection, transmission and emission spectra for DBR fiber lasers of various cavity lengths. Here, FBG_2 has been strained to produce an SLM for different cavity lengths. Moving from top to bottom and left to right, the effective cavity lengths are 1.023 m, 0.784 m, 0.538 m, 0.280 m, 0.233 m, 0.194 m, 0.158 m, 0.029 m.

The amount of strain necessary to achieve an SLM was measured as a function of cavity length by successively removing optical fiber from the center of the laser cavity. Strain was then applied to one grating (FBG_2) until an SLM was produced. The strain was calculated based on the length change exerted by the piezo stage, and the wavelength detuning of FBG_2 was measured by analyzing the transmission spectrum and calculating centroid values. The resulting wavelength shift as a function of strain was found to be 1.216 pm/με. Figure 15 shows the spectra from several lasers of varying cavity lengths. The distortion seen in FBG_2's reflection spectrum is due to absorption through the erbium fiber. In viewing the first plot, the second grating has been shifted 198 pm, a considerable amount of detuning needed for SLM operation. The laser is also operating in the sidebands of FBG_1, approximately 65 pm from the center of the grating peak. Note this laser also occasionally lased in the sidebands of the shifted grating. The combined transmission at the lasing wavelength is 5 dB, roughly 44% per grating. As noted in the caption, the effective cavity length is $\sim$1 m, all of which is erbium-doped fiber. Thus, it is possible that the marginal feedback provided at this detuning is enough to generate lasing in the sample. The next several cavity spacings exhibited similar traits, in that excessive detuning (i.e. significant spectral separation) was required to generate a SLM.

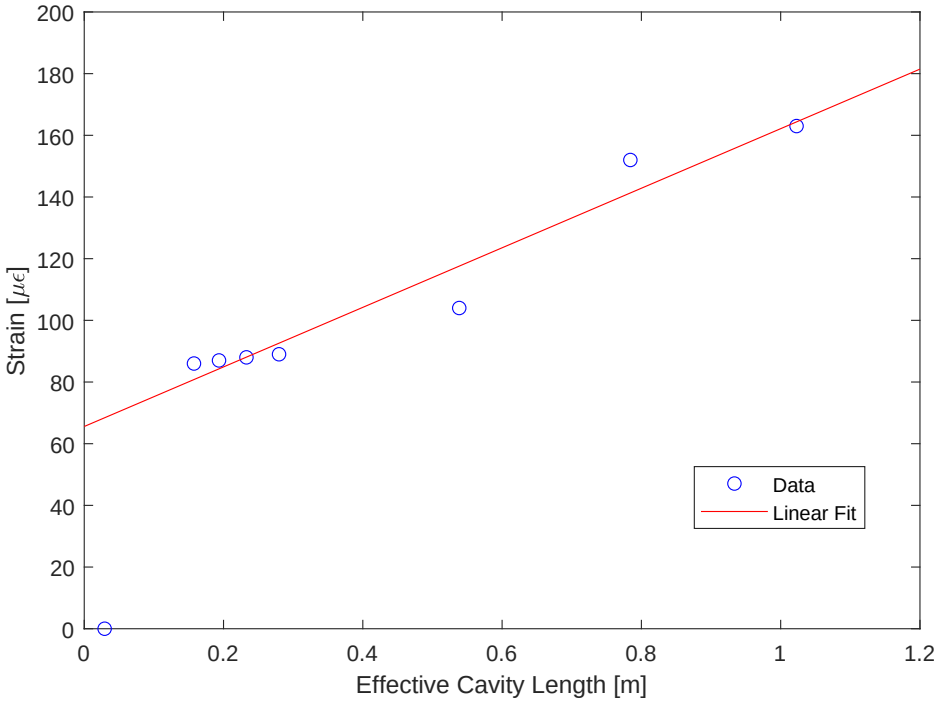

Fig. 16—Strain required to produce an SLM in DBR fiber lasers as a function of effective cavity length.

Examining the remainder of the spectra, a trend was obtained for the amount of detuning needed to facilitate lasing in a SLM. Figure 16 shows the results from the experiments, where spectral shifts have been converted to strain values. The amount of strain applied follows roughly a linear trend up until no detuning is required. Because of the difficulty in performing these measurements at shorter cavity lengths (due to cleaving and splicing), cavity lengths below 15 cm were not measured. While this data shows that single mode operation is possible over a large range of effective cavity lengths, it does not speak to the stability of the SLM operation or the amount of detuning range available to remain in an SLM. Considering the temperature sensitivity of FBGs ($\sim$12 pm/°C), a temperature swing of 0.1°C would cause one FBG to shift 1.2 pm relative to the other. For a 35 cm cavity with a longitudinal mode spacing of 2.4 pm, that amount of detuning would likely be enough to allow two modes to occupy the overlapped spectral region and prevent lasing in a SLM. This means the gratings should be packaged in a manner that is free from external strain and must experience the same temperature during operation. Otherwise, it is likely that environmental disturbances will detune the gratings enough to prevent SLM operation. Therefore, FBG packaging is critical to SLM operation when using this technique.

5.1 Laser Threshold Modeling for Cavities $>$ 16 cm

The modeling software described in previous sections was used to simulate the various cavities in an effort to understand how straining the FBGs affected the laser mode thresholds. Gratings were synthesized for each cavity to match the measured spectra (25 mm with tapered apodization profile), then one FBG was virtually strained, and the threshold values calculated. The simulated spectra along with the measured spectra are shown in Fig. 17. The first cavity (with 1 m gap between gratings) required 163 με (see caption) to achieve a spectral offset of 198 pm. As seen in the upper left plot of Fig. 17, the model matches well despite the slight difference in the bandwidth of the strained grating. This is likely due to small differences

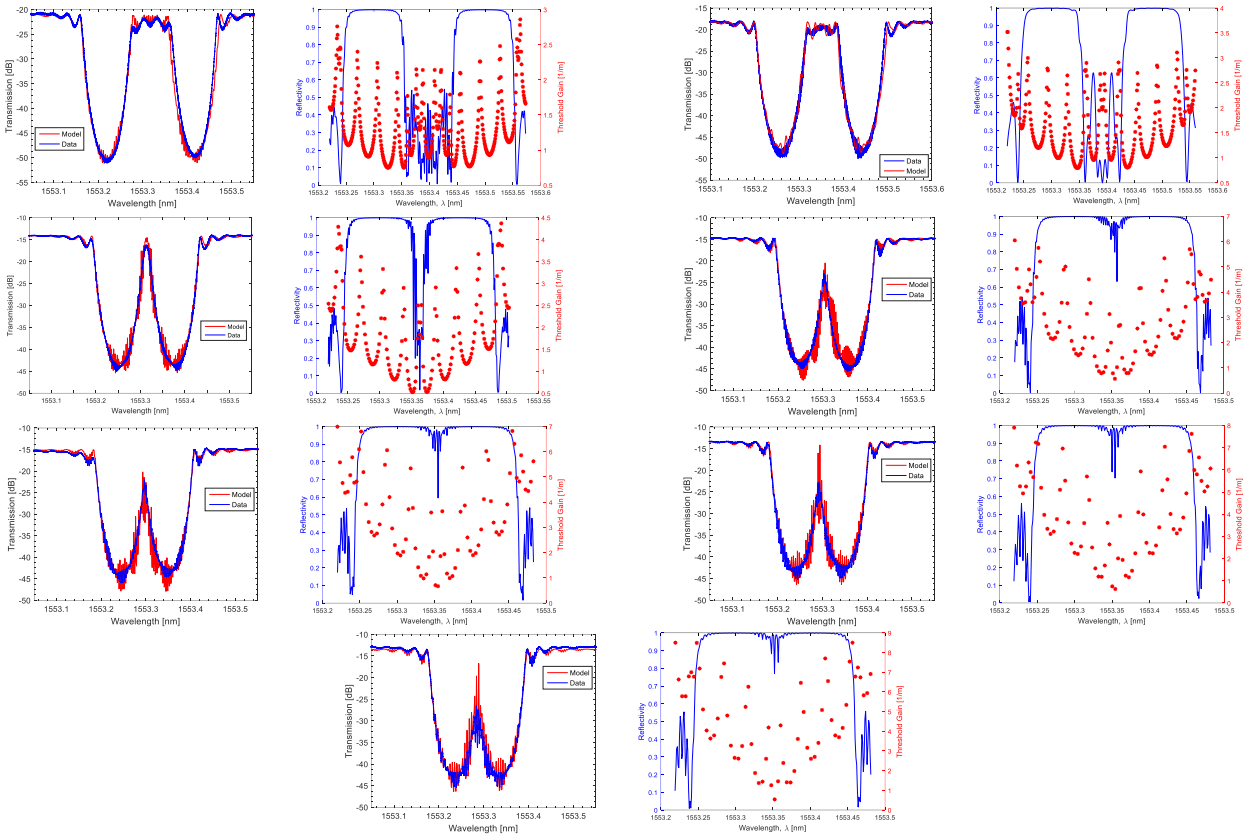

Fig. 17—(Left Plots) Simulated and measured transmission spectra. (Right Plots) Reflection spectrum and laser modes. Moving from top to bottom and left to right, the effective cavity lengths and (strain) are 1.023 m (163 με), 0.784 m (152 με), 0.538 m (104 με), 0.280 m (89 με), 0.233 m (88 με), 0.194 m (87 με), 0.158 m (86 με). Note the x-axes in the combined reflection spectrum/laser mode plots are shifted relative to the transmission spectra due to the conversion of detuning values (m^{-1}) to wavelength (nm).

between the actual grating and the modeled profile. The adjacent graph shows the calculated laser modes. Of particular note is the lobed structure of the modes. Because of the symmetry and existence of modes with similar thresholds, the model confirms that preferential lasing in one particular mode is difficult to achieve without additional selectivity added to the cavity. The graph also illustrates why SLM lasing was achieved at multiple wavelengths for this cavity length; the model predicts four locations of similar thresholds ($\sim$0.75 m^{-1}). The two lowest threshold locations (seen here as 1553.35 nm and 1553.45 nm) comprise the laser lines observed in the experiment. Other cavity lengths show similar behavior such that above a 0.5 m cavity length, the outer lobes have lower threshold values than the lobes located at wavelengths between the main Bragg resonances. This makes sense considering the grating sidelobes provide the only feedback into the cavity, resulting in an increase of the threshold values. As the cavity length decreases, the lowest threshold modes shift to the central lobe. This happens once the cavity length approaches 30 cm and the nominal strain applied to FBG_2 is about 90 με. For cavities less than 30 cm, stain values are clustered near 90 με, indicating there might be a boundary condition common to several cavity lengths.

A 3D representation of the threshold values for a laser with a 1 m cavity for different strain values applied to the second grating is shown in Fig. 18. As the grating is strained, the spectral overlap between the gratings decrease, limiting the space in which the longitudinal modes can exist. Although this model is not

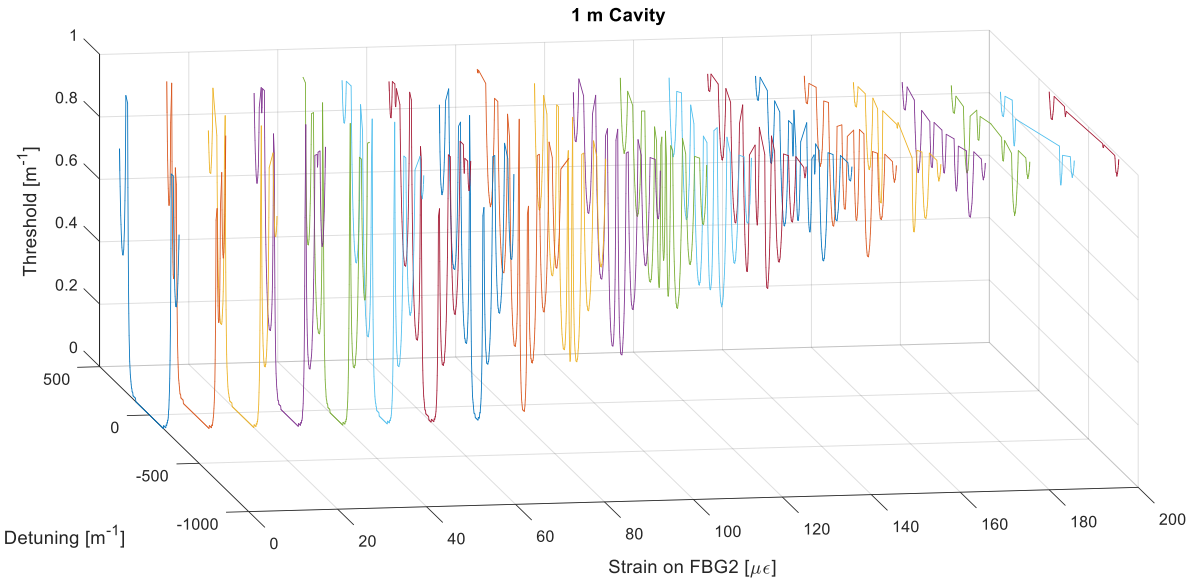

Fig. 18—Simulation of the strain applied to FBG_2 and the resulting thresholds of the various longitudinal modes.

an exact representation of the experiment—due to differing strain values and cavity length—it provides a good representation of how the laser modes evolve with applied strain. According to the model, at 80 με the lasing wavelength should be 49 pm from the center wavelength. Beyond 80 με, the minimum threshold begins to rise, the center lobe "splits," and the lowest threshold modes shift to outer lobes. At 160 με, the lowest order laser mode has been detuned 53 pm from the center wavelength. Recall that for the experimental laser, FBG_2 was strained 163 με to achieve SLM operation. Based on Fig. 18, it seems possible for stable SLM operation to occur at smaller strain values, for example at 80 με where there is a definitive minimum. Although it is unclear why lasing did not occur at this value, a possible explanation could be due the narrow longitudinal mode spacing, the higher combined reflectivity providing more optical feedback into the cavity, and the smaller lasing threshold of higher order modes.

5.2 Laser Threshold Modeling for Cavities $\leq$ 16 cm

Due to the challenges in experimentally measuring the strain required to achieve SLM operation at cavity lengths less than 16 cm, the laser software was used to simulate laser designs under varying grating parameters. Several DBR lasers with different gap lengths, grating strengths, and strain profiles were synthesized and compared. For these simulations, both gratings were 20 mm in length and utilized a tapered apodization profile. The grating strengths (κ) for FBG_1 and FBG_2 were simultaneously varied from 101 m^{-1} to 404 m^{-1}. The gap between gratings ranged from 40 mm to 160 mm, and FBG_2 was strained from 0 με to 150 με at each value of κ. For every parametric combination, the number of modes was calculated using the "available gain" criterion described previously. The results of the simulations are illustrated in Fig. 19. The graphs show the number of modes (represented by contours) as a function of the applied strain to FBG_2 and coupling strength of the gratings (left plots). The plots can additionally be stacked vertically to generate a volumetric representation of the entire mode space as a function of strain, coupling strength, and cavity length (see Fig. 20). This permits the evolution of the mode fronts to be easily viewed as the cavity length increases. Figure 20 also shows the laser thresholds for the lowest order modes at each cavity length.

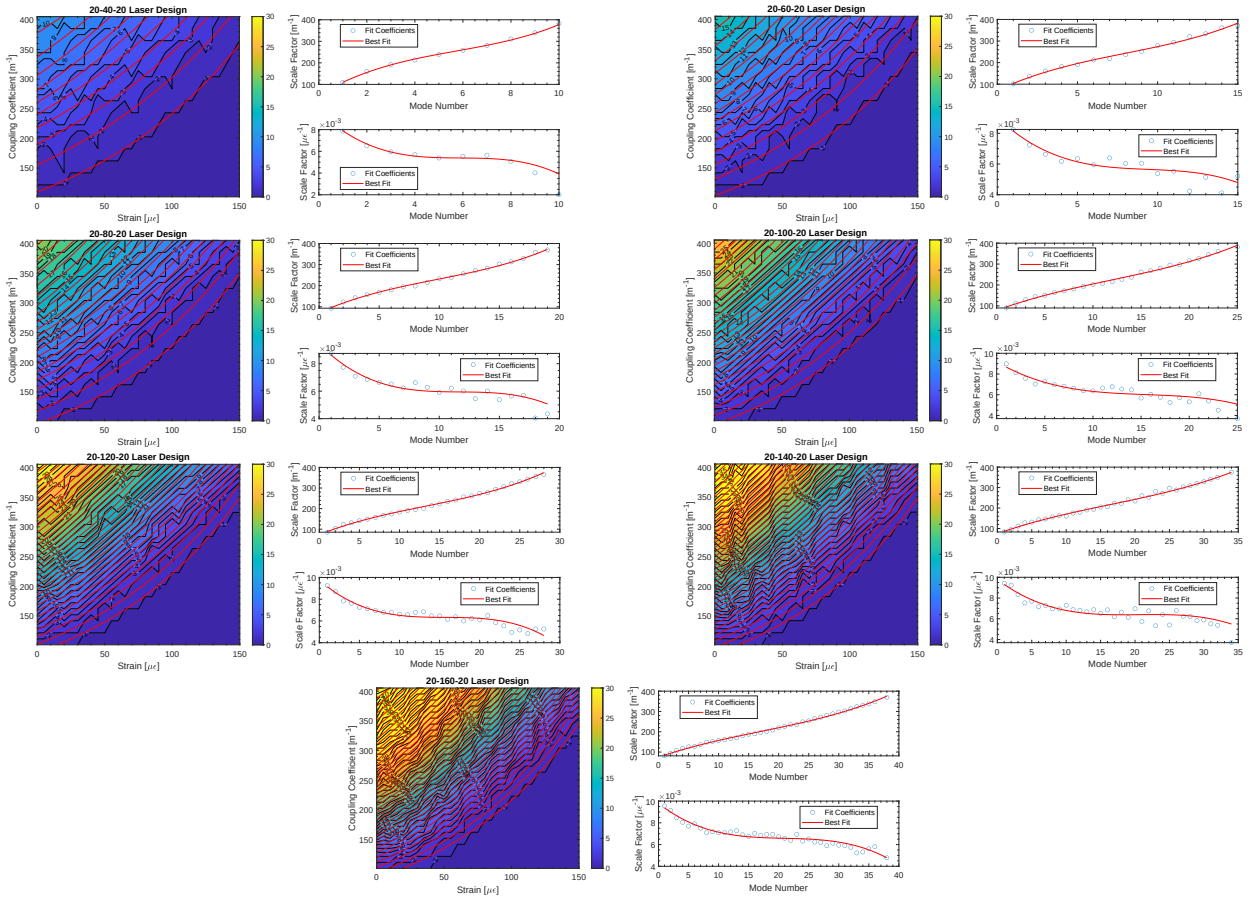

Fig. 19—(Left Plots) Contour plot representing the number of modes as a function of strain and coupling coefficient. Red lines represent fits to the contours using $f(x) = ae^{bx}$ and the parameters derived from the plots to the right. (Right Plots) Fit coefficients used to derive the mode contours. The top graph represents the a coefficient; the bottom graph, b. Moving from top to bottom and left to right, the cavity lengths are 40 mm, 60 mm, 80 mm, 100 mm, 120 mm, 140 mm, and 160 mm.

Each modal front in Fig. 19 was fit to a exponential equation of the form $f(x) = ae^{bx}$. The coefficients a and b (open circles in right plots) were then fit to 3$^{\text{rd}}$ order polynomials as a function of mode number. These fit parameters were next used as an initial guess to generate an optimized solution evaluating all mode fronts simultaneously. The global solution is depicted as the red lines in both plots. As expected, the longer the cavity length, the more tightly packed the mode fronts. This can easily be seen by contrasting the first and last plots (40 mm and 160 mm) in Fig. 19, where the longitudinal mode spacing of the 160 mm allows more modes to fit within the grating bandwidths. The mode contours are quasi-linear and become more linear as the mode number increases. The estimated fits follow the mode fronts well for cavity lengths below 80 mm. At 80 mm and beyond, the fit tends to incorrectly predict the strain required at low to moderate strain values. Some of this error is attributed to the coarseness of the simulation performed; the κ values were increased in increments of 20 m^{-1}, corresponding to a 1×10^{-5} change in the index modulation, and the strain values were sampled at increments of 5 με. While the sampling values could be improved, doing so increases the computational time by a factor of 20 for one data set (6.5 hours on a Xeon core processor with ample memory).

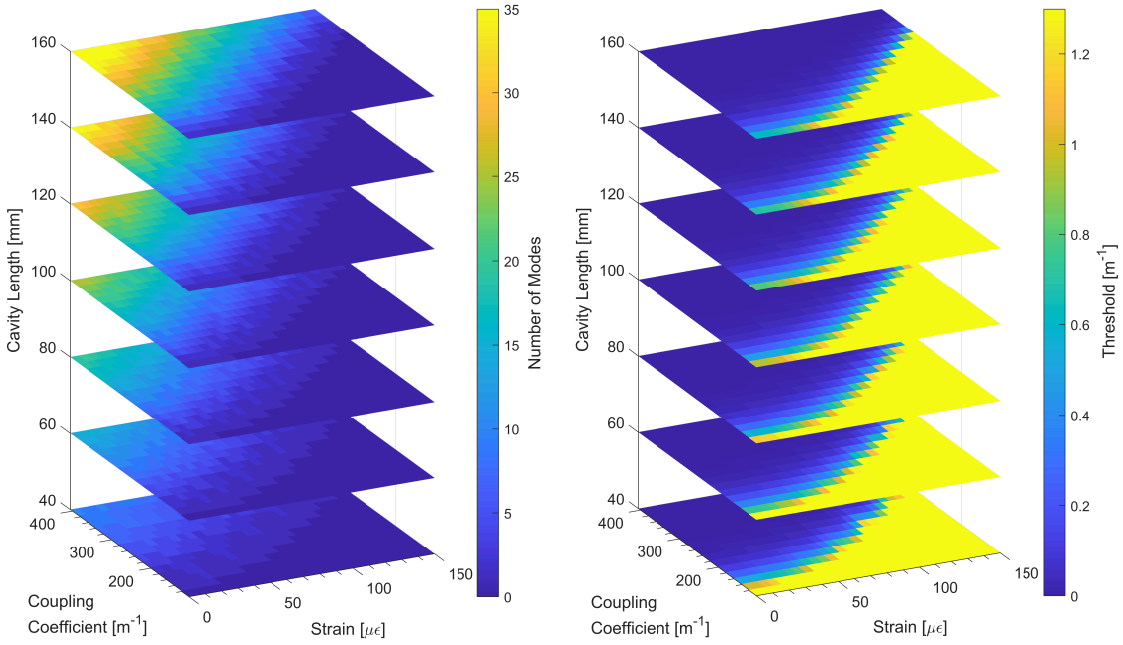

Fig. 20—Stacked representation of the (Left) simulated data in Fig. 19 and the (Right) laser thresholds of the lowest order modes as a function of applied strain, coupling coefficient, and cavity length.

To explore quantization effects, a simulation was run using a more densely populated parameter space. The top graph in Figure 21 illustrates the mode structure for the 80 mm cavity with fine and coarse sampling of the parameters. In the left plot, the κ values were increased by 5 m^{-1}, and the strain values were sampled at increments of 1 με. The plot to the right shows the coarse sampling data set used in Fig. 19. In comparing the intensity plots, it is clear that the mode contours are not only smoother and more regular in the finely sampled figure but also contain a highly detailed structure. Specifically, the graph depicts scalloped contours in the higher order modes (most notably, mode 2). The behavior can potentially be explained by examining the transmission spectrum of the laser under two strain conditions near these regions. Using a peak κ value of 162 m^{-1}, the laser was simulated with 38 με and 46 με strain applied to FBG_2. As illustrated in Fig. 21, the two spectra show a distinct difference in the lobes formed by the Fabry-Perot resonances. The 38 με spectrum exhibits a centered resonance flanked by two equally strong lobes. This spectrum corresponds to the mode 1 regions between the sharp dips of mode 2. The other spectrum displays a centrally-located lobe surrounded by equally strong resonances. This spectrum is produced when FBG_2 is strained by 46 με, within a dip region. Because these resonance conditions repeat, the mode fronts exhibit the periodic structure observed in the top figure. The single, centrally-located resonance in the first spectrum is indicative of lasing in an SLM. The second spectrum on the other hand provides two equally likely modes for the laser to operate. The presence of this other mode creates instability in the laser due to mode competition, increases the lasing thresholds, and decreases the output power per mode. The laser thresholds for combinations that produce an SLM in the Nufern fiber are shown in the bottom graph of Fig. 21. The plot illustrates how the threshold of the SLM decreases as the grating strength increases and the operating conditions move closer to the mode 2 contour.

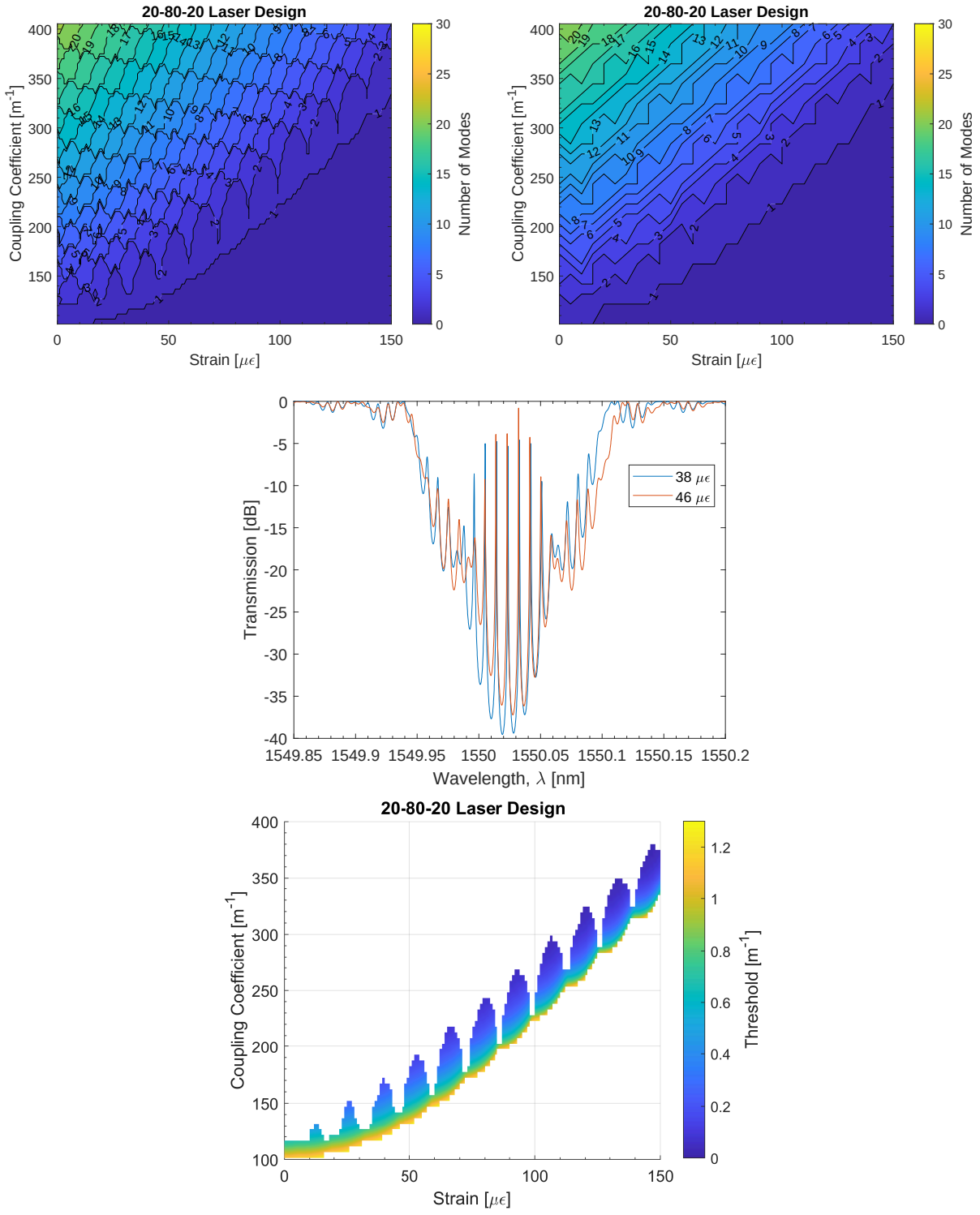

Fig. 21—Contour plot representing the number of modes as a function of strain and coupling coefficient for an 80 mm cavity with (Top Left) fine and (Top Right) the original coarse sampling. (Middle) Transmission spectra for gratings with a κ of 162 m^{-1} under two strain conditions. (Bottom) Laser thresholds for single longitudinal modes under various strain and coupling coefficient combinations.

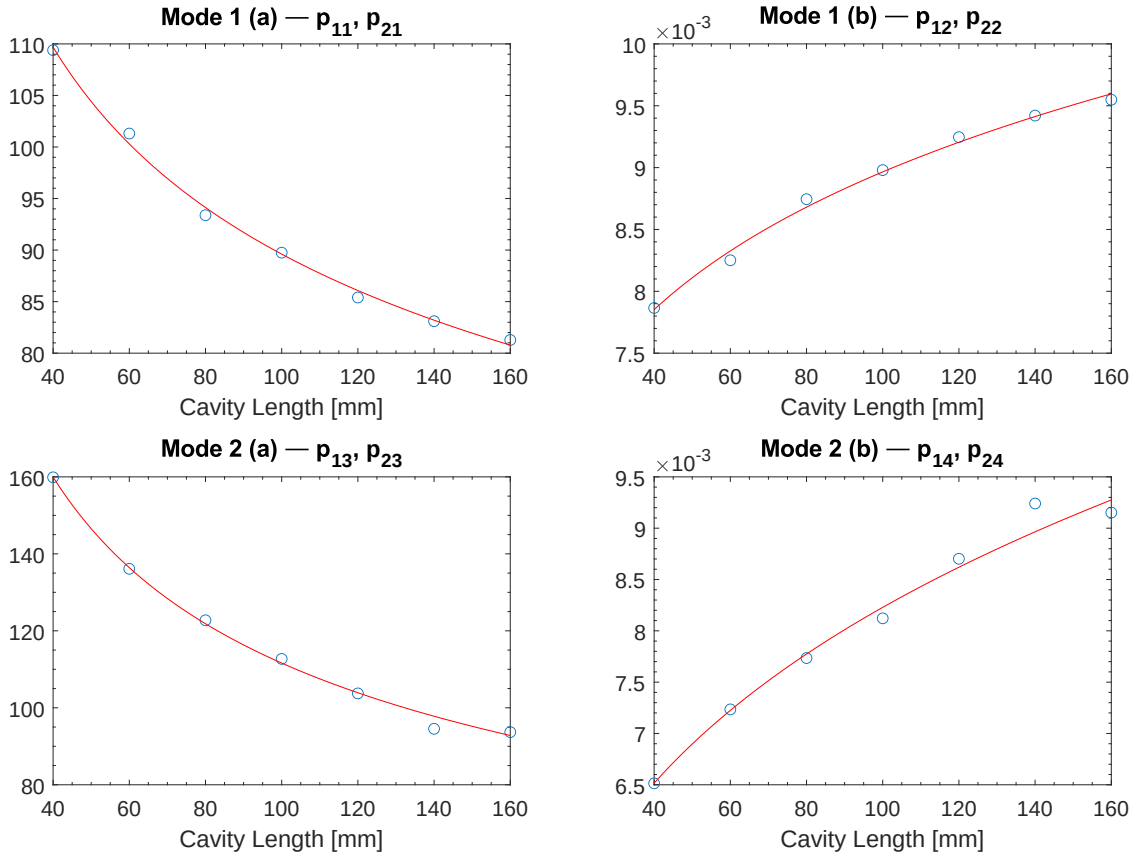

Fig. 22—Fit coefficients for modes 1 and 2 versus cavity length. (Top Left and Right) Mode 1 (Bottom Left and Right) Mode 2.

Since SLM operation is dictated by the functional dependence of the lowest order modes, a revised equation was found by fitting the first and second mode contours over all cavity lengths. The updated expression involved using a power law function to represent the coefficients a and b in the exponential equation described above. The new formula was then used to estimate the laser behavior for various cavity designs. The form of the new equation is given by

$$\begin{aligned} \kappa_1 &= p_{11} {L_c}^{p_{21}} \exp(p_{12} {L_c}^{p_{22}} \varepsilon) \quad \text{for mode 1,} \\ \kappa_2 &= p_{13} {L_c}^{p_{23}} \exp(p_{14} {L_c}^{p_{24}} \varepsilon) \quad \text{for mode 2.} \end{aligned} \tag{6}$$

Table 1—Power Law Fit Parameters for Modes 1 and 2

p_{xx}	1	2	3	4
1	247.47	0.004603	680.84	0.002547
2	-0.2206	0.1447	-0.3926	0.2547

where p_{xx} represents a fit coefficient, L_c is the cavity length, and ε is the applied strain. The best fits to the coefficients for modes 1 and 2 are depicted in Fig. 22. The generalized coefficients, a and b, are denoted in

parentheses while the power law coefficients are designated by p_{xx}. The fit coefficients are found in Table 1. Equation (6) can be used to develop a simple criterion to determine whether a laser design will produce a SLM (assuming two 20 mm gratings of equal strength). A solution can be found by numerically computing a family of solutions depending on the parameter being investigated. For example, if a specific cavity length (L_c) and strain value (ε) are known, Eq. (6) can be evaluated directly to find κ values that will lase in a SLM. Then, the following criteria can be used:

$$\begin{array}{l} \kappa > \kappa_2, \text{ 2 or more modes} \\ \kappa_2 \geq \kappa \geq \kappa_1, \text{ 1 mode} \\ \kappa < \kappa_1, \text{ 0 modes.} \end{array} \tag{7}$$

Similarly, a range of ε values can be calculated to match a known κ to estimate the strain needed to keep the laser in a SLM. This can be accomplished by calculating the ICC, typically a value of 7 for a well-behaved laser. The ICC is found by multiplying the resultant κ by the length of the gratings and the apodization factor (if the FBGs are apodized). Since the laser cavity is defined by two gratings, this number is then doubled. Using an apodization factor of 0.9 and an FBG length of 20 mm, the peak coupling coefficient is 194 m^{-1}. Numerically solving Eq. (6) for a cavity length of 80 mm yields a minimum strain value of 60 με to produce a SLM. If the laser model is used to calculate the minimum strain for SLM operation, a value of 57 με is determined, illustrating that the approximation is in good agreement with the established model.

Alternatively, the κ values for modes 1 and 2 can be averaged to find the range of coupling coefficients that lie on the centerline between the modes, giving the highest probability of achieving an SLM laser. This was accomplished by averaging the local fits for mode 1 and 2 (designated as mode 1.5) and fitting the simulated data to the function used in Eq. (6) over all cavity lengths. The resultant equation is

$$\kappa_{1.5} = p_{11} {L_c}^{p_{21}} \exp(p_{12} {L_c}^{p_{22}} \varepsilon) \quad \text{for mode 1.5,} \tag{8}$$

where the new fit parameters are listed in Table 2. Equation (8) can then be used to determine strain values that provide the widest latitude in maintaining an SLM.

Table 2—Fit Parameters

p_{xx}	1	2
1	441.42	0.003343
2	-0.3194	0.2046

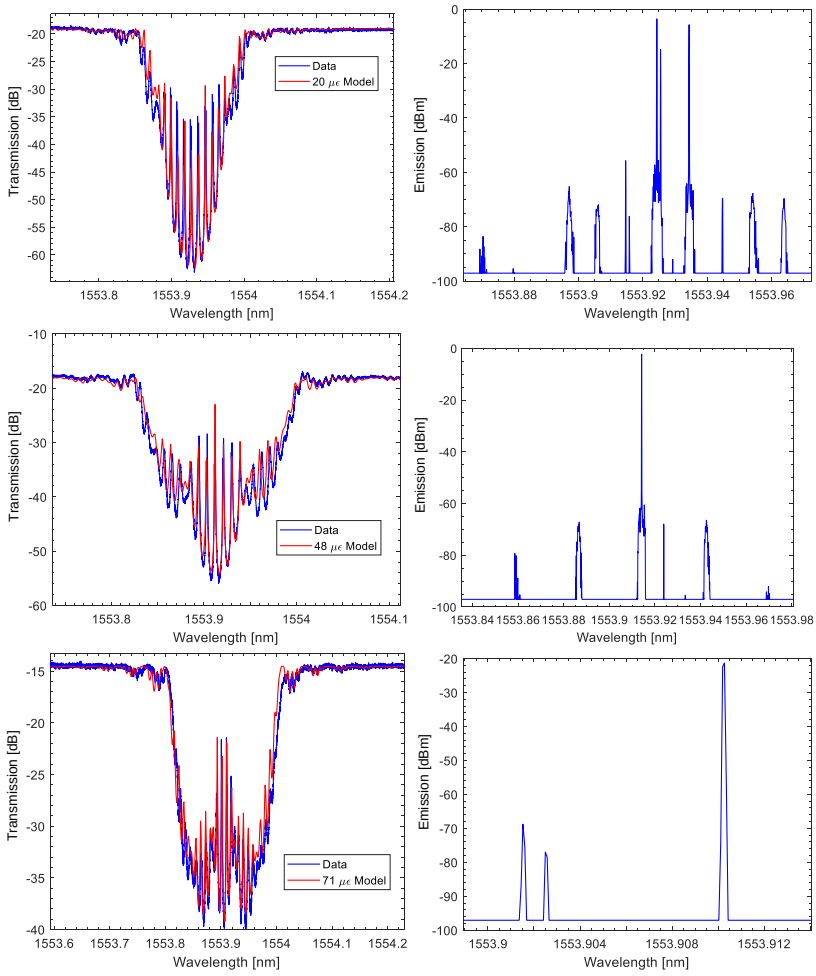

Fig. 23—(Left) Transmission and (Right) emission spectra for a 20-80-20 DBR laser where FBG_2 has been strained by (Top) 20 με, (Middle) 48 με, and (Bottom) 71 με.

5.3 Experimental

To verify the simulations, a DBR laser was fabricated and subjected to a series of strain measurements to observe the SLM behavior. The design employed a 20-80-20 mm structure, with 20 mm FBG lengths and a gap length of 80 mm. The gratings were apodized with a tapered cosine function and inscribed at a scan speed of 0.075 mm/s. The resultant gratings exhibited transmissions depths around 21 dB. The average tension during the fabrication of FBG_1 was approximately 30 g while FBG_2 was written with 20 g of tension. The transmission spectrum for the laser is shown in Fig. 23. Modeling the laser revealed a refractive index change of 8×10^{-5} with a maximum kappa of 161.7 m^{-1}. The total transmission measured by the Apex OSA was 43.7 dB. As illustrated in the top plot, the model indicates the two gratings were offset by 24 pm, requiring 20 με of strain to be virtually applied to FBG_2. The emission spectrum measured by the OSA is plotted to the right in Fig. 23. The figure shows two distinct longitudinal modes and one polarization mode present. The longitudinal modes are separated by 10.03 pm, giving an effective cavity length of 83.03 mm. Simulations of the laser cavity estimate 3 modes using the "available gain" criterion.

Next, FBG_2 was strained until an SLM was obtained. According to the model, 48 με (Middle in Fig. 23) of applied strain was required to prevent higher order modes from lasing. The emission spectrum shows a

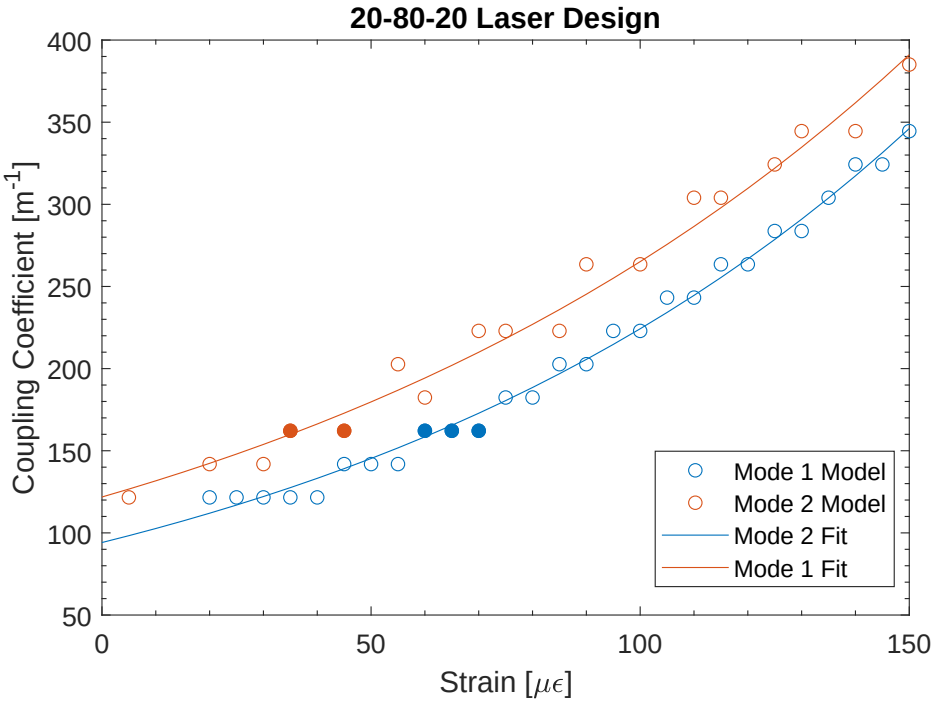

Fig. 24—(Open Circles) Modes 1 and 2 for a DBR laser with an 80 mm cavity as calculated by the laser model. (Closed Circles) Mode combinations with a κ value of 162 m^{-1}. (Lines) Mode fronts calculated using Eq. (6).

strong SLM with almost 0 dBm of optical power and a higher order mode suppression $>$ 60 dB. The grating was then strained until an SLM was no longer supported. Based on modeling, the last value of ε to achieve an SLM was 71 με (Bottom in Fig. 23). From the plot, the maximum transmission is around 25 dB, about the minimum combined grating strength needed for lasing to occur. Modeling showed that the threshold was 1.21 m^{-1}, providing rationale to the 20 dB drop in optical power over the previous case (especially since the maximum gain in the fiber is 1.3 m^{-1}). Based on these measurements, the tuning range available for SLM operation was about 20 με, comprising a spectral shift of 24 pm for FBG_2. In terms of temperature sensitivity, this equates to $\pm$ 1 °C.

The measurements were also used to test the analytical expressions displayed in Eq. (6). Recall that the gratings had a peak κ value of 162 m^{-1}. For an apodization of 0.9 and a length of 20 mm, the ICC of two gratings is 5.83. Using Eq. (6), mode 2 ends at about 37 με, and mode 1 cuts off around 63 με (mode 1.5 is 50 με). Considering the experimental data showed SLM lasing between 48 με and 71 με, a potentially large error exists in the estimations provided by the analytical expressions. Fortunately, this discrepancy can be understood by examining the simulation of the 20-80-20 laser design in more detail. Figure 24 illustrates the mode fronts for modes 1 and 2 as calculated by the laser model (open circles) and the analytical expressions (lines). The closed circles in the plot indicate modes supported by gratings with κ values of 162 m^{-1}. According to the plot, mode 2 actually cuts off at 45 με and mode 1 at 70 με. Since the lines to not actually capture all combinations of mode solutions but instead utilize a least squares fit through the points, Eq. (6) is unable to precisely describe the tuning range of the SLM. Instead, it can only provide an quick estimate of possible strain values. Note that using the more densely sampled simulation in Fig. 21, an SLM may be supported under two strain conditions, 38 με to 43 με, and 48 με to 70 με.

6. CONCLUSIONS

To help predict the performance of different laser designs, a numerical model was utilized to solve for the modes of DBR fiber lasers. The model was successfully used to simulate the response of linear cavity resonators to changes in the cavity length, grating reflectivities, and tuning of the gratings. For model verification, extended laser cavities employing Fabry-Perot resonators were fabricated with cavity lengths up to 1 m. Comparison of the model to experimental data showed good agreement, where differences could be accounted for by approximations made in the model, instrument resolution, dynamic range, and sampling. Discrepancies also arose from phase and amplitude errors imparted during grating inscription not incorporated into the model. Experiments were also conducted to determine how the longitudinal mode structure varied depending on the amount of gain available in the laser cavity and where the gain medium was placed within the cavity. As expected the output power and number of modes increased as the length of erbium fiber increased. In another series of experiments, the effect of grating reflectivity and bandwidth on the number of modes supported by a linear cavity laser was measured. Measurements showed that the number of modes decreased with reflectivity in a linear fashion. To determine how the bandwidth alone affected the number of modes, several gratings of different lengths were written, then spliced onto the laser cavity. Results showed a roughly linear relationship between the number of modes and the bandwidth of the second grating. When the grating was sufficiently strong, a divergence between the laser model and the data set was noted. This was largely due to the grating sidelobes having enough reflectivity to support lasing at those wavelengths. These experiments were invaluable in confirming the laser model's validity, providing confidence in the modeling software to simulate various laser designs.

To achieve SLM operation in an extended cavity DBR fiber laser, one grating was spectrally offset from the other, reducing the spectral overlap between the gratings and limiting the bandwidth. Detuning of the grating was accomplished by applying strain to one FBG. Using this approach, SLM operation of various laser cavities was achieved and their performance characterized. Simulations and experiments found that for long cavities (> 50 cm), lasing could occur in the sidelobes of gratings. The model was then utilized to simulate lasers with cavities less than 16 cm. Mode contours were fit and analytical expressions were found that estimated the performance of the lasers. Discrepancies between experimental data and the analytical fit were explained by coarse sampling of the parameters in the simulations and the loss of legitimate solutions outside the least squares fit. For short cavities, the permissible detuning range for one grating is on the order of ± 1 °C, allowing for realistic deployment of these lasers as sensors. For lasers using longer cavities, mitigation of temperature differentials is necessary to achieve continuous SLM operation.

ACKNOWLEDGMENTS

Funding for this project was provided by the 6.2 NRL base program. The laser threshold modeling algorithm was adapted from code provided by Geoffrey Cranch (NRL Code 5675).

REFERENCES

1. Y. O. Barmenkov, D. Zalvidea, S. Torres-Peiró, J. L. Cruz, and M. V. Andrés, "Effective length of short Fabry-Perot cavity formed by uniform fiber Bragg gratings," *Opt. Express* **14**(14), 6394–6399 (Jul 2006), doi:10.1364/OE.14.006394.

2. G. A. Miller, "Decrease in Photosensitivity of Erbium-Doped Fiber Under Tension: Implications for Distributed Feedback Fiber Lasers," *J. Lightwave Technol.* **36**(14), 3040–3045 (Jul 2018).

3. T. Erdogan, "Fiber grating spectra," *Journal of Lightwave Technology* **15**(8), 1277–1294 (Aug 1997), ISSN 0733-8724, doi:10.1109/50.618322.

4. T. Makino, "Threshold condition of DFB semiconductor lasers by the local-normal-mode transfer-matrix method: correspondence to the coupled-wave method," *Journal of Lightwave Technology* **12**(12), 2092–2099 (Dec 1994), ISSN 0733-8724, doi:10.1109/50.350622.

5. L. Rodríguez-Cobo, M. A. Quintela, S. Rota-Rodrigo, M. López-Amo, and J. M. López-Higuera, "Single-longitudinal mode laser structure based on a very narrow filtering technique," *Opt. Express* **21**(8), 10289–10294 (Apr 2013), doi:10.1364/OE.21.010289.

6. W. H. Press, S. A. Teukolsky, W. T. Vetterling, and B. P. Flannery, *Numerical Recipes 3rd Edition: The Art of Scientific Computing*, 3 ed. (Cambridge University Press, New York, NY, USA, 2007).

7. J. Skaar, "Synthesis and characterization of fiber Bragg gratings," 2000.

8. G. A. Miller and H. M. Coombs, "Low Loss Splices to Dissimilar Optical Fibers," *NRL Memorandum Report* **NRL/MR/5675–18-9822** (Nov 2018). URL `https://apps.dtic.mil/dtic/tr/fulltext/u2/1064067.pdf`.

9. G. A. Miller, G. M. H. Flockhart, and G. A. Cranch, "Technique for correcting systematic phase errors during fibre Bragg grating inscription," *Electronics Letters* **44**(24), 1399–1400 (November 2008), ISSN 0013-5194, doi:10.1049/el:20081896.

10. G. A. Miller, J. R. Peele, C. G. Askins, and G. A. Cranch, "Characterization of strong fiber Bragg gratings using an applied thermal chirp and iterative algorithm," *Appl. Opt.* **50**(36), 6617–6626 (Dec 2011), doi:10.1364/AO.50.006617.

11. G. A. Miller, "Measurement of UV-induced Birefringence by Thermal Annealing of a Distributed Bragg Reflector Fiber Laser," *NRL Memorandum Report* **NRL/MR/5675–18-9831** (Jan 2019). URL `https://apps.dtic.mil/sti/pdfs/AD1066327.pdf`.